Journal of Flow Chemistry (2021) 11:143–162
https://doi.org/10.1007/s41981-020-00121-6

FULL PAPER

Electrosynthesis of 3,3′,5,5′-Tetramethyl-2,2′-biphenol in Flow

Maximilian Selt[1,2] · Barbara Gleede[1] · Robert Franke[3,4] · Andreas Stenglein[1] · Siegfried R. Waldvogel[1,2]

Received: 23 September 2020 / Accepted: 13 October 2020 / Published online: 1 December 2020

Abstract

3,3′,5,5’-Tetramethyl-2,2′-biphenol is well known as an outstanding building block for ligands in transition-metal catalysis and is therefore of particular industrial interest. The electro-organic method is a powerful, sustainable, and efficient alternative to conventional synthetic approaches to obtain symmetric and non-symmetric biphenols. Here, we report the successive scale-up of the dehydrogenative anodic homocoupling of 2,4-dimethylphenol (**4**) from laboratory scale to the technically relevant scale in highly modular narrow gap flow electrolysis cells. The electrosynthesis was optimized in a manner that allows it to be easily adopted to different scales such as laboratory, semitechnical and technical scale. This includes not only the synthesis itself and its optimization but also a work-up strategy of the desired biphenols for larger scale. Furthermore, the challenges such as side reactions, heat development and gas evolution that arose during optimization are also discussed in detail. We have succeeded in obtaining yields of up to 62% of the desired biphenol.

Keywords Electrosynthesis · Oxidation · Phenol · Anode · Biphenol · Sustainable synthesis

Introduction

Biphenols are an important structural motif in organic chemistry as they are part of many natural products and pharmaceuticals [1–8]. The outstanding importance of biphenols is probably due to their use as ligand building blocks in transition metal catalysis [9–11]. A particular representative of this is 3,3′,5,5’-tetramethyl-2,2′-biphenol (**5**). Therefore, the biphenol is used e.g. as phosphonamidite or phosphite ligands for the copper [12–15] or rhodium-catalyzed [16–18] asymmetric addition reaction of alkyl radicals to double bonds. Further applications are the palladium-catalyzed Heck alkylation [19] or the asymmetric allylic alkylation reaction [20]. In particular, **5** is of tremendous importance as ligand building block in the hydroformylation reaction (Scheme 1) [21–23]. This is one of the most important fields in technical homogeneous catalysis (Production of 10.4 Mt/a oxo chemicals in 2008) [21]. The industrial relevance of biphenols and thus **5** is evident.

The synthesis of **5** is achieved by direct oxidative homocoupling of 2,4-dimethylphenol (**4**) (Scheme 2). This transformation can be realized by conventional chemical methods either by using stoichiometric or over-stoichiometric amounts of oxidants [25–29]. Or by using transition metal catalysts, such as rhodium(III) metallocene [30], $VO(acac)_2$ [31], $RuCl_3$ [32] and many more [33, 34]. However, these methods suffer from low yield and moderate selectivity and additionally generate large amounts of reagent waste. Further preparation takes place. In addition, the catalysts or oxidants used are usually expensive and toxic. In summary, the conventional chemical processes for the synthesis of **5** are unecological and show poor economic efficiency. Alternative synthesis routes are therefore urgently needed.

Especially, in the view of current global challenges such as climate change and scarcity of resources, green and renewable technologies are increasingly in the focus of the chemical

Highlights
- Dehydrogenative anodic homocoupling of 2,4-dimethylphenol to 3,3′,5,5′-Tetramethyl-2,2′-biphenol.
- Investigations of an electrochemical synthesis of 3,3′,5,5′-Tetramethyl-2,2′-biphenol, which is of technical interest.
- Development of an electrochemical procedure with focus on optimization and scale-up in different flow electrolysis cells.

✉ Siegfried R. Waldvogel
waldvogel@uni-mainz.de

[1] Department of Chemistry, Johannes Gutenberg University Mainz, Duesbergweg 10-14, 55128 Mainz, Germany

[2] Material Science in Mainz (MAINZ) Graduate School of Excellence, Staudingerweg 9, 55128 Mainz, Germany

[3] Evonik Performance Materials GmbH, Paul-Baumann-Straße 1, 45772 Marl, Germany

[4] Lehrstuhl für Theoretische Chemie, Ruhr-Universität Bochum, 44780 Bochum, Germany

Scheme 1 Twofold hydroformylation of 1,3-butadiene [24]

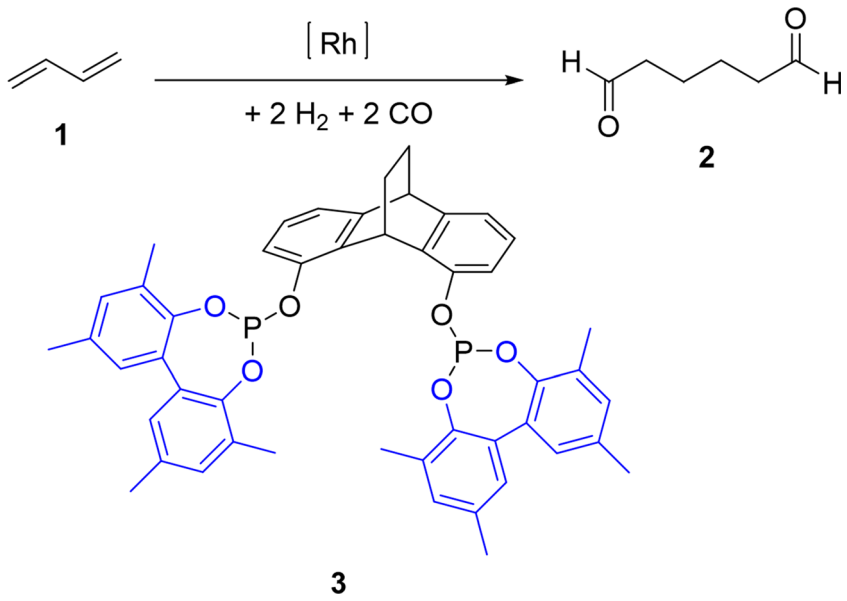

industry [35–40]. This demand can be covered by electro-organic synthesis as this is in-line with "green chemistry" [41–44]. In contrast to classical chemical processes, the activation occurs reagent-less by electric current. Thus, mostly toxic, and/or expensive oxidants or reducing agents and transition metal catalysts can be avoided [45, 46]. Consequently, reagent waste is circumvented. Moreover, electrochemical syntheses are more atom-economical because new synthesis routes are enabled with fewer synthetic steps and without pre-functionalization of the precursors. In addition, electrochemistry is inherently safe and superior to classical methods. For example, it is not necessary to use highly reactive or explosive oxidizers, the reaction is often carried out under mild conditions, and in an emergency the reaction can be stopped by simply switching off the power supply. If electricity from renewable sources is used, electrochemical processes also help to stabilize the electrical grid [47]. Therefore, it is not surprising that electrochemistry has become extremely relevant. The recently emerged organic electrosynthesis is being adopted in both academia and industry as the twenty-first century's synthetic technique [48–59].

In 1973, when Nilsson et al. worked on the development of an electrochemical hydroxylation of phenols, they discovered the first electrochemical synthesis of **5** by direct dehydrogenative oxidative homocoupling of **4** [60]. Using a lead oxide anode and aqueous sulphuric acid as solvent they were able to obtain **5** in a yield of moderate 30% as a side-product. The electrosynthetic approach to **5** was a major field of Waldvogel group within the past decades [48, 61]. Under most conditions this particular substrate **4** is very prone to side reactions and forms polycyclic products in a broad structural diversity [62–65]. Consequently, a boron-templated anodic process was established which provides good yields even on multi-kg scale [66, 67]. However, this was a multi-step procedure and generates borate containing waste-water [68]. Several approaches were able to provide the desired **5** in a direct electrosynthesis but only in moderate yields [69–71]. This electrolysis was adopted and further developed in the Waldvogel group. The yield was successfully increased up to 60% by using graphite as anode material and 1,1,1,3,3,3-hexafluoropropan-2-ol (HFIP) as solvent [71]. This example shows the specific influence of HFIP, which is known for its

Scheme 2 Electrochemical synthesis of 3,3′,5,5'-tetramethyl-2,2′-biphenol (**5**) by direct dehydrogenative oxidative homocoupling of 2,4-dimethylphenol (**4**).

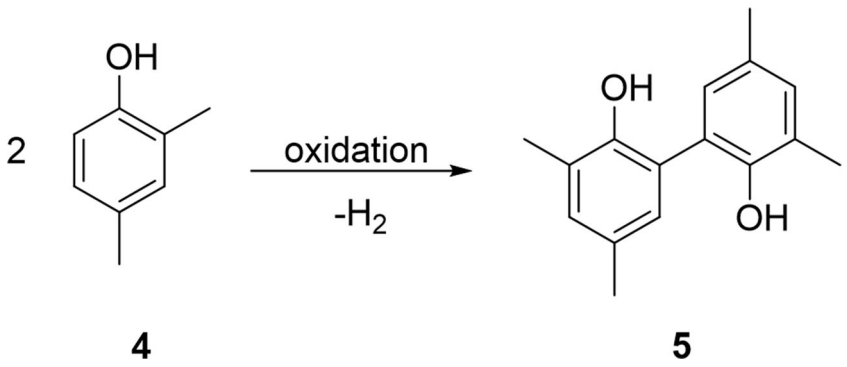

ability to stabilize radicals and cations [72–74]. Additionally, it is characterized by high polarity, low nucleophilicity and excellent hydrogen bond donor properties [74, 75]. Due to its high redox stability, which results in combination with the electrode material BDD in an outstanding large electrochemical window of 5 V, HFIP is particularly well suited for electrochemical coupling reactions of phenols and arenes [76–78]. In cross-coupling reactions, HFIP is also the key to selectivity, as it ensures decoupling of oxidation potential and nucleophilicity of the used starting material [79]. New results based on molecular dynamics simulations show that HFIP and HFIP-water as well as HFIP-alcohol mixtures have a unique microheterogeneous structure [80, 81]. The separation of the polar hydroxyl groups from the fluorinated groups lead to domain formation, which positively influences electrochemical coupling reactions. On the one hand, the solvation on the intermediates is improved by facilitating the hydrogen bonding formation of the polar domains. On the other hand, the adsorption of the starting materials onto the electrode surface is promoted. This is because the system aims to minimize the repulsive fluorine-lipophilic interaction and maximize the attractive hydrophobic interaction. This increases the local concentration of starting materials at the electrode surface and facilitates the electron transfer of the starting material to the electrode. Another effect of microheterogeneity is a very low viscosity of the solution. This results in a positive effect on the mass transfer during electrolysis and can make processes more robust [80, 81].

A challenge in the synthesis of **5** is the large number of side reactions that can occur depending on the chosen reaction conditions [61]. In addition, the over-oxidations of **5** always leads to the formation of oligomers and polymers. A further aspect that is becoming increasingly interesting is the scale-up of the synthesis of **5** in a technical scale. Especially, regarding the development of a technically relevant process, experiments on a technical or semi-technical scale are indispensable. The first steps in this direction have already been successfully accomplished. We could already publish first results in the beaker-type cell using glassy carbon electrodes and very common and inexpensive bromide-containing supporting electrolytes [61, 82]. In addition, a supporting electrolyte-free method was developed as flow electrolysis and scaled-up to the semi-technical scale using the 4 cm × 12 cm electrolysis cell equipped with a glassy carbon anode and a stainless steel cathode. As alternative for a solid supporting electrolyte pyridine was added to provide a sufficient conductivity. After optimization of the reaction an isolated yield of 58% of **5** was obtained [83]. Especially, the continuous process of flow chemistry offers many advantages for scale-up, whereas batch processes are limited to a few liters' reaction volume [84–94]. Moreover, it simplifies the heat management and the surface-to-volume ratio of the electrode is superior compared to batch electrolysis. In this manuscript we show the scale-up of the electrochemical synthesis of **5** in the flow cell up to technical scale.

Results and discussion

In this section the development of the electrosynthesis of **5** in a flow electrolysis cell scaled-up to the technical scale is reported. On basis of the scaled beaker-type cell electrolysis (Scheme 3) [82], a successive approach was chosen to convert the synthesis into a flow process: For the transfer of the reaction from a batch to a flow process the 2 cm× 6 cm flow electrolysis cell developed for laboratory scale was used [21]. The electrolysis was than scaled-up. Initially, to the semi-industrial scale using the developed 4 cm × 12 cm electrolysis cell. The process was then scaled-up to the technical scale using the "EUT Pilot cell". In addition, the various challenges, e.g. heat development, conductivity, and hydrogen evolution, that occur during scale-up are discussed.

Transfer to flow electrolysis cell

For the transfer of the electrosynthesis of **5** in the 2 cm × 6 cm flow electrolysis cell, the already optimized conditions of the beaker-type cell electrolysis were chosen (Scheme 3): [82] The electrolysis of **4** was carried out in HFIP with 15 vol.% of water and the use of tetraethylammonium bromide (Et_4NBr) as supporting electrolyte at a temperature of 50 °C. Et_4NBr was chosen as supporting electrolytes because tetraalylammonium bromides generally give the best yield of **5** in this system and is the most inexpensive compound of the tested supporting electrolytes. By adding water to the electrolyte bromination as side-reaction can be suppressed effectively. Glassy carbon was used as electrode material for both electrodes. A slight excess of charge of 1.2*F* was added to obtain the most complete conversion to the desired **5**. The applied current density of 6.1 mA/cm^2 was moderate.

Based on the results from the investigated batch electrolysis [82], initial experiments were carried out in the 2 cm × 6 cm flow electrolysis cell (Fig. 1). For this purpose, the optimized conditions from the batch electrolysis were adopted mostly. However, the current density was reduced by half to 3 mA/cm^2 and, since the flow electrolysis cell did not allow temperature control, the electrolysis was performed at room temperature. The yield was determined by gas chromatography and internal standard calibration, as this made the optimization more time efficient (yield*). The result of this first experiment was rather insufficient: Only a yield* of 27% was achieved (Table 1, Entry 1), which is very low compared to the isolated yield of 46% achieved in the 25 mL beaker-type electrolysis cell (25 mmol phenol) [82]. The change from a batch to a flow process is not trivial and makes a significant difference in reaction control.

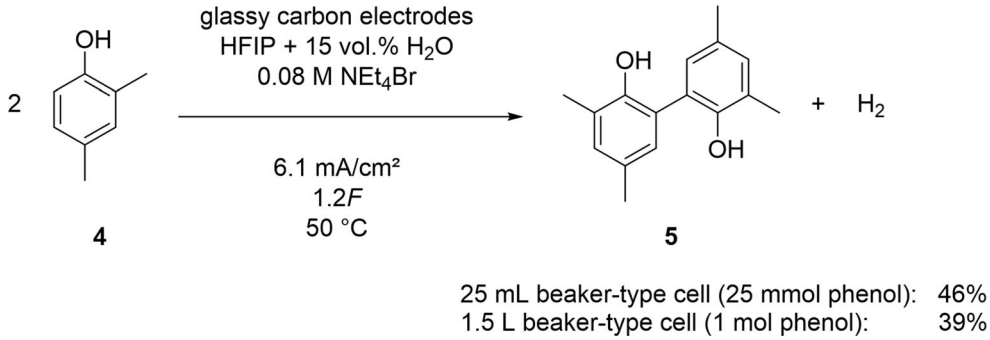

Scheme 3 Electrolysis conditions of the dehydrogenative homocoupling of **4** in the 25 mL (25 mmol phenol **4**) and 1.5 L beaker-type cell (1 mol phenol **4**) [82]

Therefore, the synthesis was optimized. The starting conditions for the optimization (Table 1, Entry 2) are based on reaction conditions that have already been successfully used for electrochemical cross-coupling reactions in the Waldvogel group [82, 95–97]. In addition, BDD was selected as the anode because it shows an excellent performance in cross-coupling reactions. Stainless steel was chosen as cathode material, due to its cost efficiency and stability using it as cathode [98]. Another reason for the choice of these electrode materials was that the "EUT pilot cell", which was later to be used on a technical scale, is only equipped with BDD anodes and stainless steel cathodes. Therefore, BDD and stainless steel were already used at the beginning of the development process. First, the influence of adding additives such as methanol or water was investigated to avoid the brominating of the product, when using bromine-containing supporting electrolyte [82]. In the past, we could show that the addition of methanol is very advantageous for cross-coupling reactions [79]. For this study, 18 vol.% methanol (Table 1, Entry 3) and 15 vol.% water (Table 1, Entry 4) were added to the solvent HFIP. However, for the synthesis of **5**, the use of pure HFIP is best suited (Table 1, Entry 2), even if the formation of brominated by-products cannot be completely suppressed.

Next, the current density was investigated in the range of 2.4–45 mA/cm^2 (Supporting information 5.1). In summary, the electrolysis is very robust and can tolerate even high current densities of up to 45 mA/cm^2. Using higher current densities has two effects on the electrolysis. First, the electrolysis time can be significantly reduced, which makes the whole process more time efficient. Second, there is an increased heat development. Nevertheless, the electrolysis can be carried out up to 45 mA/cm^2 without a cooling system in the used setup. A similar yield* of the desired product (24% **5**) is obtained using 40 mA/cm^2 instead of 2.4 mA/cm^2 (Table 1, Entry 5). The next parameter was the applied charge Q. For this purpose, several experiments were carried out in a range from 0.25–3.25 F (Fig. 2). The yield* of **5** increases in the range of 0.25–1.00*F*, because below 1.00*F* not enough electrons are available for a complete conversion. In the range of 1.00–2.00*F* a plateau is reached. Here the yield* does not increase further, but starting material is still being converted, which means that mainly by-products are formed. At higher charge quantities, the yield* of **5** also decreases. This can be explained by the over-oxidation of the product and the formation of oligomeric and polymeric structures of **5**. It is therefore important to use the theoretically necessary applied charge of 1.00*F* (Table 1, Entry 6). This results in two advantages: Over-oxidation and the formation of by-products are suppressed, which facilitates the processing and protects the consumption of the starting material (unreacted starting material can be recovered by distillation after electrolysis and fed back to the process). Furthermore, a better current yield is achieved, and the process is therefore more current efficient.

Table 1 Optimization in the 2 cm × 6 cm flow electrolysis cell

Entry	c(**4**) [$\frac{mol}{L}$]	Solvent	c(Supporting electrolyte) [$\frac{mol}{L}$]	Q [*F*]	j [$\frac{mA}{cm^2}$]	T [°C]	Electrode material	d [cm]	ν [$\frac{mL}{min}$]	Yield* **5**
1	1.0	HFIP +15 vol.% H_2O	Et_4NBr 0.08	1.1	3.0	22	GC||GC	0.025	0.02	27%
2	0.5	HFIP	Et_4NBr 0.08	1.2	2.4	22	BDD||SS	0.05	0.03	28%
3	0.5	HFIP +18 vol.% MeOH	Et_4NBr 0.08	1.2	2.4	22	BDD||SS	0.05	0.03	20%
4	0.5	HFIP +15 vol.% H_2O	Et_4NBr 0.08	1.2	2.4	22	BDD||SS	0.05	0.03	17%
5	0.5	HFIP	Et_4NBr 0.08	1.2	40.0	22	BDD||SS	0.05	0.03	24%
6	0.5	HFIP	Et_4NBr 0.08	1.0	40.0	22	BDD||SS	0.05	0.60	23%
7	0.5	HFIP	$MeBu_3NO_3SOMe$ 0.005	1.0	40.0	20	BDD||SS	0.05	0.60	43%

Electrolysis conditions: anode area: 12 cm^2. Applied charge refers to **4**. Q: applied charge. j: current density. T: temperature. d: interelectrode gap. ν: flow rate. GC: glassy carbon. BDD: boron-doped diamond. SS: stainless steel. *Yield determined by calibrated GC

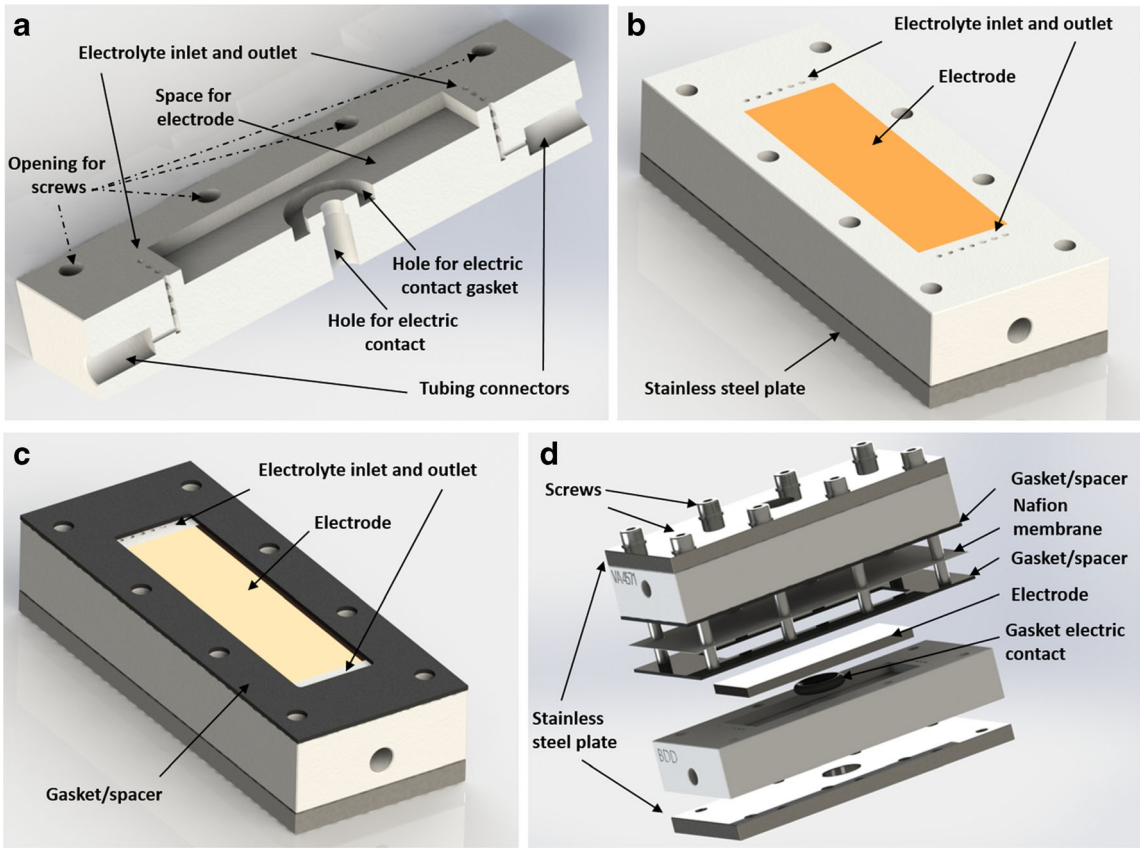

Fig. 1 Technical drawings of 2 cm × 6 cm flow electrolysis cell: **a** Cross-section of the Teflon piece with connection for tubing, inlet, outlet and free space for electrode. **b** Complete half-cell containing Teflon piece, the electrode (yellow) and a stainless steel plate. **c** Half-cell with gasket/spacer on top. **d** Exploded drawing of a complete divided flow electrolysis cell. For the undivided mode, the Nafion membrane and one gasket/spacer is omitted. The electrochemical 2 cm × 6 cm flow cell is commercially available as *ElectraSyn flow* (IKA Werke). Reprinted with permission from [21]. Copyright [2020] American Chemical Society

A challenge with electrolysis is the heat generation at high current densities already mentioned above. To avoid excessive heating of the electrolyte, a temperature-controlled cathode was used in the following. The stainless steel block used for this purpose has a meandering cooling channel inside that can be connected to an external cooling system (Supporting information 2.1, Fig. S1). This made it possible to control the temperature of the electrolysis cell. With this adaption, different supporting electrolytes and their concentration were examined for their suitability. In addition to NEt_4Br, methyltributylammonium methyl sulfate ($MeBu_3NO_3SOMe$) and methyltriethylammonium methyl sulfate ($MeEt_3NO_3SOMe$) were used as supporting electrolyte. $MeEt_3NO_3SOMe$ was chosen because it has already been successfully used in various homo- and cross-coupling reactions [70, 71, 96]. However, this supporting electrolyte is not commercially available and must first be synthesized by reacting the highly toxic compounds triethylamine and dimethyl sulfate [96]. Therefore, $MeBu_3NO_3SOMe$ was also tested as a further supporting electrolyte, which is also a known supporting electrolyte for electrochemical phenol coupling and, moreover, does not have to be produced at great effort and expense [97]. For each of the three supporting electrolytes the concentration was initially varied between 0.02 and 0.24 mol/L (Fig. 3). Especially, at low concentrations of supporting electrolyte, the possibility of cell cooling becomes

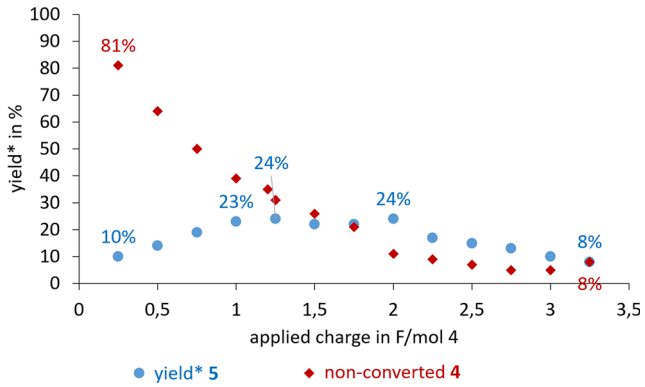

Fig. 2 Optimization of applied charge Q in a range of 0.25–3.25*F* per mole **4**: Yield* of **5** in blue and unconverted **4** in red. Electrolysis conditions: 0.5 mol/L 2,4-dimethylphenol (**4**), 0.08 mol/L NEt_4Br, HFIP, BDD||stainless steel, anode area: 12 cm^2, current density j: 40 mA/cm^2, flow rate: 0.18–2.39 mL/min, interelectrode gap: 0.05 cm, 22 °C. *Yield determined by calibrated GC

more important since the lower conductivity of the electrolyte increases the terminal voltage and thus the heat development. For this reason, the following electrolysis were kept to 20 °C.

Here it became clear that all three investigated supporting electrolytes behave similarly: The lower the supporting electrolyte concentration, the higher the yield* of **5**. The greatest effect can be observed with NEt_4Br, with which a yield* of 40% was achieved at a concentration of 0.02 mol/L, and only a yield* of 15% at 0.24 mol/L. Less severe, but still similar, is the effect with $MeEt_3NO_3SOMe$ (0.02 mol/L: 37%, 0.24 mol/L: 25%) and $MeBu_3NO_3SOMe$ (0.02 mol/L: 36%, 0.24 mol/L: 18%). The reason for this behavior is presumably the occupancy of the electrode surface: When a potential is applied, the supporting electrolyte cations move to the cathode according to the electric field, the supporting electrolyte anions to the anode. If the supporting electrolyte concentration is now very high, the electrode surface is occupied by the corresponding supporting electrolyte ions. This makes it increasingly difficult for the phenol to meet the electrode surface and to release an electron there. The yield* decreases accordingly.

Following this trend, the supporting electrolyte concentration was then further reduced to 0.0025 mol/L (Fig. 4). If the yields* at 0.01 mol/L (Fig. 4, NEt_4Br: 42%, $MeBu_3NO_3SOMe$: 43% and $MeEt_3NO_3SOMe$: 44%) are compared with those at 0.02 mol/L (Fig. 4, NEt_4Br: 40%, $MeBu_3NO_3SOMe$: 36% and $MeEt_3NO_3SOMe$: 37%), a slight increase in yield* can be seen. However, a further lowering of the supporting electrolyte concentration does not lead to any significant improvement. On the contrary, if only 0.0025 mol/L supporting electrolyte is used, the terminal voltage increases very strongly (~70 V, device maximum reached), which on the one hand makes a reproducible electrolysis with the voltage source used impossible and on the other hand also results in a very high energy consumption. At a supporting electrolyte concentration of 0.005 mol/L the terminal voltage is only approx. 30 V and electrolysis can be carried out without any problems. Although higher supporting electrolyte concentrations lead to a further decreasing of the terminal voltage, a supporting electrolyte concentration of 0.005 mol/L is favored regarding the economic efficiency of the process due to the application costs and easier processing. Comparing the yields* of the different supporting electrolytes at 0.005 mol/L, $MeEt_3NO_3SOMe$ gives the best result with 45% yield* for **5**. However, the yield* using $MeBu_3NO_3SOMe$ (43%) is only slightly lower and this supporting electrolyte does not have to be synthesized since it is technically available. Furthermore, unlike NEt_4Br, no brominated by-products are formed. Therefore, 0.005 mol/L $MeBu_3NO_3SOMe$ was used as supporting electrolyte in the following (Table 1, Entry 7). In summary, the enormous effect of the reduced supporting electrolyte concentration should be pointed out: The yields* were increased from initially 23% to 43%.

As already mentioned above, a lowering in the supporting electrolyte concentration leads to an increase in the terminal voltage. To counteract this, the electrode gap has been reduced from the previous 0.05 cm to 0.025 cm and 0.012 cm. As expected, the average terminal voltage drops from 38 V at an electrode gap of 0.05 cm to 12 V at 0.012 cm. However, the highest yield* of 48% was at an electrode gap of 0.025 cm. To explain this, another effect must be considered: In addition to the phenol coupling on the anode side, there is a counter-reaction on the cathode side. This is mainly the reduction of protons to hydrogen. The cathodically generated gas leads to the problem that it takes up a not inconsiderable part of the cell volume and thus disturbs the anode reaction [99]. If small interelectrode gaps are used, the cell volume is smaller, and the disturbing influence of hydrogen increases accordingly. Larger electrode spacings reduce this influence.

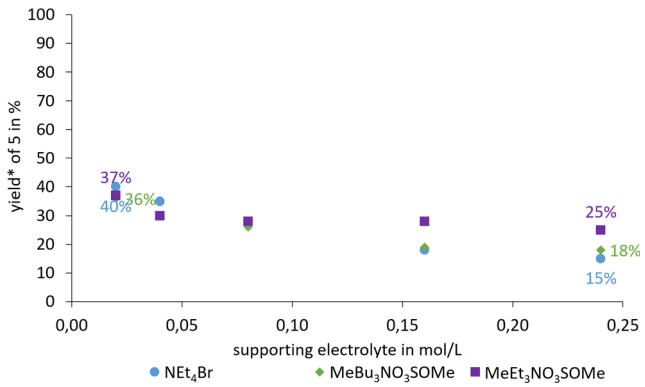

Fig. 3 Yield* of **5** for different concentrations of NEt_4Br (blue), $MeBu_3NO_3SOMe$ (green) and $MeEt_3NO_3SOMe$ (purple). Electrolysis conditions: 0.5 mol/L 2,4-dimethylphenol (**4**), 0.02–0.24 mol/L supporting electrolyte, HFIP, BDD||stainless steel, anode area: 12 cm^2, current density: 40 mA/cm^2, applied charge: 1.0*F*, flow rate: 0.6 mL/min, interelectrode gap: 0.05 cm, 20 °C. *Yield is determined by calibrated GC

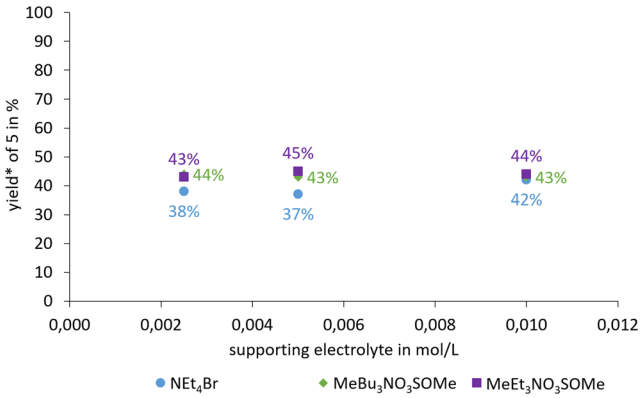

Fig. 4 Yield* of **5** for different concentrations of NEt_4Br (blue), $MeBu_3NO_3SOMe$ (green) and $MeEt_3NO_3SOMe$ (purple). Electrolysis conditions: 0.5 mol/L 2,4-dimethylphenol (**4**), 0.0025–0.0100 mol/L supporting electrolyte, HFIP, BDD||stainless steel, anode area: 12 cm^2, current density: 40 mA/cm^2, applied charge: 1.0*F*, flow rate: 0.6 mL/min, interelectrode gap: 0.05 cm, 20 °C. *Yield determined by calibrated GC

Accordingly, two factors that influence the performance of electrolysis in opposite directions are involved here, namely the terminal voltage and the cathodic hydrogen evolution. The mean interelectron gap of 0.025 cm was a compromise between these two factors, which also produced the highest yield* of 48%. In addition, an attempt was made to completely dispense with supporting electrolyte at each of the three electrode spacings, but in all three cases the terminal voltage was too high for electrolysis to be carried out. Even the addition of 1 vol.% – 20 vol.% by volume of trifluoroacetic acid (TFA) or methanol instead of a supporting electrolyte did not lead to any improvement, so that supporting electrolyte cannot be completely dispensed with (Supporting information, 5.1). However, a concentration of 0.005 mol/L $MeBu_3NO_3SOMe$ is very low and the economic efficiency of the process is ensured.

At the beginning of the reaction optimization the current density was investigated. However, due to the strong heat development at high current densities, the range of the investigated area was limited to a maximum of 45 mA/cm^2. Since it was now possible to cool the cell, the current density range under investigation was extended to a maximum value of 80 mA/cm^2 (Supporting information, 5.1). The yields* of **5** are relatively constant up to 60 mA/cm^2. At higher current densities, the yield* decreases slightly. This extends the current density window even further: The electrolysis can be operated with current densities between 2.4 mA/cm^2 and 60 mA/cm^2. This has two advantages. Firstly, the operation of a (flow) electrolysis at high current densities is preferable, since this allows a better space-time yield to be achieved. Secondly, the wide range of possible current densities allows a high degree of flexibility of the process, which is particularly advantageous regarding coupling electrolysis on a technical scale with renewable energies. If an energy excess is available, the electrochemical plant can be started up and operated at high current densities. If there is a temporary shortage of energy, production is reduced. In this way, a contribution can be made to stabilize the electricity grid [47]. It should also be emphasized that such robustness is extremely rare for electro-organic transformations. As a rule, normally these only occur within a very narrow window at low current densities (0.5–5 mA/cm^2) [100–103]. Apart from the electrochemical C-C coupling [104] there are only a few examples, e.g. the Kolbe electrolysis [105] or the Baizer process, [106] which also show such robustness.

Next, electrolysis was carried out at temperatures of 10 °C to 50 °C. Since the amount of heat generated during electrolysis depends on the current density, the temperature screening was carried out at a current density of 40 mA/cm^2 and 60 mA/cm^2 (Fig. 5). Hereby it can be investigated how a temperature change can have an influence on the reaction and thus on the process flow if the current density is changed dynamically. At a current density of 40 mA/cm^2 (Fig. 5, blue), it has been shown that 20 °C was already the optimum temperature and provides a yield* of 47%. On one hand, higher temperatures generally lead to a lower viscosity of the electrolyte and thus to an improvement in mass transfer. Additionally, higher temperatures lead to an increase in conductivity. On the other hand, however, they have a negative influence on the homocoupling of **4**. The interaction of high temperature and the heat generated by applying high current densities results in uncontrolled boiling of the electrolyte, especially on the electrode surface. This becomes particularly clear in the case of electrolysis at 60 mA/cm^2 (Fig. 5 green), as here active cooling to 10 °C is required to prevent yield* losses. This made it possible to achieve a yield* of 50%.

The challenge of hydrogen evolution has already been addressed in the context of optimizing the interelectrode gap. In addition to increasing the cell volume, an increase in the flow rate is one way of counteracting this problem, since the hydrogen produced is then removed from the cell volume more quickly. However, it must be noted that the individual parameters are interlinked in a flow electrolysis and cannot be considered independently of each other. Thus, an increase in the flow rate is always associated with a decrease in the amount of charge. There are different possibilities to keep the applied charge constant at higher flow rates. Either the current density must be increased so that the same number of electrons can still be withdrawn when the dwell time in the cell is shortened. The way the electrolyte passes through the cell must be elongated. Other possibilities are that the electrolysis is carried out either in the form of a cascade (Fig. 6) or with a recirculation approach. The resulted applied charge can be kept constant by pumping the electrolyte through the cell several times at a high flow rate. In a cascade reaction this is done by pumping the electrolyte several times successively through the cell: In a two-step cascade, for example, the flow rate is doubled compared to the single-step process, thus halving the amount of

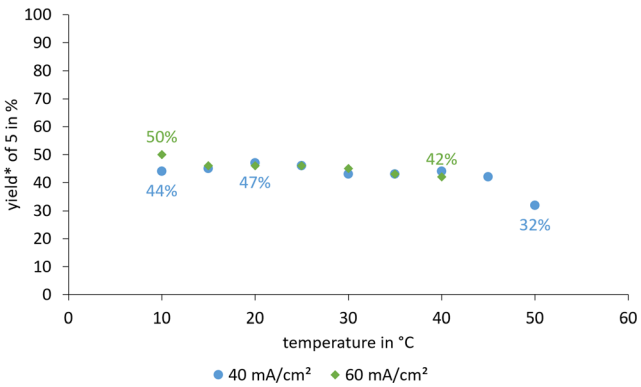

Fig. 5 Yield* of **5** for different temperatures. Electrolysis conditions: 0.5 mol/L 2,4-dimethylphenol (**4**), 0.005 mol/L $MeBu_3NO_3SOMe$, HFIP, BDD||stainless steel, anode area: 12 cm^2, current density: 40 mA/cm^2 (blue) and 60 mA/cm^2 (green), applied charge: 1.0*F*, flow rate: 0.6 mL/min and 0.9 mL/min, interelectrode gap: 0.025 cm. *Yield determined by calibrated GC

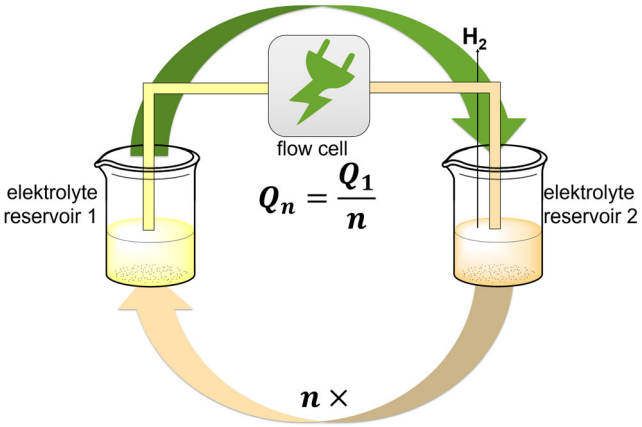

Fig. 6 Schematic representation of a cascade electrolysis. The electrolyte is pumped $n\times$ successively from electrolyte reservoir 1 through the flow electrolysis cell into electrolyte reservoir 2 at a flow rate $\nu_n = n \times \nu_1$, where ν_1 is the flow rate for a single step electrolysis. In this way only a part $Q_n = \frac{Q_1}{n}$ of the applied charge for a single step electrolysis Q_1 is applied in each step. After each step, the electrolyte is transferred from electrolyte reservoir 2 to electrolyte reservoir 1

charge applied in one step. Accordingly, the electrolyte must be pumped through the electrolysis cell twice in succession to maintain the desired charge quantity at the end of the process. In contrast, with the recirculation approach, the electrolyte is pumped at increased flow rates in a circle through the flow cell until the necessary amount of charge has been introduced into the electrolyte. In preliminary studies the recirculation approach was tested for a similar system but did not lead to better yields.

Therefore, the electrosynthesis of **5** was conducted in form of a cascade, initially at 40 mA/cm^2, with two, four and ten-steps (Table 2). The positive effect of this electrolysis mode is very impressive. With an increasing number of cascade steps, the yield* increases until finally, with a ten-step cascade, a yield* of 60% could be achieved.

As the last parameter, the starting material concentration was varied between 0.5 mol/L and 2.0 mol/L (Supporting information, 5.1). These experiments were also carried out in the form of a ten-step cascade. It was found that the concentration of the starting material in the tested area had no influence on the yield*, as it was constant at 60%. Nevertheless, the use of a high starting material concentration of 2.0 mol/L of **4** is advantageous for the electrolysis: Both solvent and supporting electrolyte can be saved and processing is facilitated, since more product is formed per volume of electrolyte.

Finally, the optimized conditions were applied to a cascade electrolysis at 60 mA/cm^2. A constant yield* of 61% was also obtained here. Due to the reaction optimization carried out in the 2 cm × 6 cm flow electrolysis cell, the yield* was significantly increased from initially 27% to 61%. As mentioned above, all optimization work was done using yields with internal calibration (yield*). After successful optimization, the product was isolated by column chromatography and a isolated yield of 62% for **5** was obtained. In comparison to the previously developed supporting electrolyte-free system using pyridine as additive (isolated yield of 58% in the 2 cm × 6 cm flow electrolysis cell) the yield is slightly higher when using a supporting electrolyte [83]. The optimized reaction conditions are summarized in Table 6, Entry 2.

Scale-up in the semi-technical scale

Based on the optimization in the 2 cm × 6 cm flow electrolysis cell (anode area: 12 cm^2), the reaction was scaled-up. For this purpose, the 4 cm × 12 cm flow electrolysis cell, which was developed in the Waldvogel group recently, with an anode area of 48 cm^2 was used (Fig. 7) [107]. As previous experiments with the 4 cm × 12 cm electrolysis [83] cell have shown that an increased energy or heat input into the electrolyte is to be expected due to the larger electrode area, the electrolysis conditions optimized for the 2 cm × 6 cm electrolysis cell were initially slightly modified: Cooling to 10 °C was applied at the lower current density of 40 mA/cm^2 and an interelectrode gap of 0.050 cm was selected. With these adaptations an isolated yield of 55% could be obtained (Table 3, Entry 1).

Subsequently, the electrode gap was reduced to 0.025 cm, which was accompanied by an increase in isolated yield to 57% (Table 3, Entry 2). Finally, the current density was also increased to 60 mA/cm^2. Thus, with the optimized parameters, an isolated yield of 58% could be achieved (Table 3, Entry 3), which is very similar to the isolated yield of 59% for the supporting electrolyte-free process [83]. This shows that electrosynthesis of **5** can be scaled without major yield losses either with or without supporting electrolyte.

Table 2 Cascade reactions in the 2 cm × 6 cm flow electrolysis cell

Entry	Number of cascade steps	Q [*F*]	Q for each cascade step [*F*]	ν [$\frac{mL}{min}$]	Yield* **5**
1	1	1.00	1.00	0.60	48%
2	2	1.00	0.50	1.19	49%
3	4	1.00	0.25	2.39	51%
4	10	1.00	0.10	5.97	60%

Electrolysis conditions: 0.5 mol/L 2,4-dimethylphenol (**4**), 0.005 mol/L $MeBu_3NO_3SOMe$, HFIP, BDD‖stainless steel, anode area: 12 cm^2, current density: 40 mA/cm^2, applied charge: $n \times \frac{1{,}0\ F}{n}$, interelectrode gap: 0.025 cm, 20 °C. Q: applied charge. ν: flow rate. *Yield determined by calibrated GC

Table 3 Optimization of the electrochemical synthesis of 5 using the 4 cm × 12 cm flow electrolysis cell

Entry	j [$\frac{mA}{cm^2}$]	d [cm]	ν [$\frac{mL}{min}$]	Yield **5**
1	40	0.050	5.97	55%
2	40	0,025	5.97	57%
3	60	0,025	8.95	58%

Electrolysis conditions: 2.0 mol/L 2,4-dimethylphenol (**4**), 0.005 mol/L $MeBu_3NO_3SOMe$, HFIP, BDD‖stainless steel, anode area: 48 cm^2 , applied charge: 10 × 0, 1 F, 10 °C. Number of cascade steps: 10. j: current density. d: interelectrode gap. ν: flow rate. Isolated yields

In general, scale-up is possible without scaling effects. However, it is important that the cell geometry does not change too much. In the case of the 2 cm × 6 cm or 4 cm × 12 cm flow electrolysis cell, the anode area increases from 12 cm^2 to 48 cm^2, but the width-to-length ratio of 1:3 remains constant. Thus, scale-up could be realized quickly and easily without major loss in yield (Table 6, Entries 2 and 3).

Scale-up to the technical scale

For the technical relevant application, the successful scale-up in the technical scale of an electrochemical process is very important. For this purpose, Eilenburger Elektrolyse- und Umwelttechnik GmbH (EUT) provided a pilot cell for the technical scale (EUT pilot cell, Fig. 8) to transfer the synthesis of **5**. The cell is designed as a bipolar cell with two compartments and has a total electrode area of 312 cm^2. A BDD anode and a stainless steel cathode are installed in each of the two compartments. The electrodes can each be cooled from the backside via an external cooling circuit.

Slightly modified, milder reaction conditions were also initially selected for the transfer of the reaction from the medium scale of the 4 cm × 12 cm flow electrolysis cell to the EUT pilot cell. Thus, instead of 0.005 mol/L $MeBu_3NO_3SOMe$, 0.020 mol/L $MeBu_3NO_3SOMe$ was used for the first experiment. The reason was that a bipolar cell was now used instead of a monopolar one. The voltage of bipolar cells behaves additively with an increasing number of compartments, which is why an increased terminal voltage was generally to be expected. To not get into the range of the voltage maximum of the power supply (150 V), the conductivity of the electrolyte was increased by a higher concentration of the supporting electrolyte. In addition, work was carried out at 40 mA/cm^2 and 10 °C to prevent excessive heating of the electrolyte due

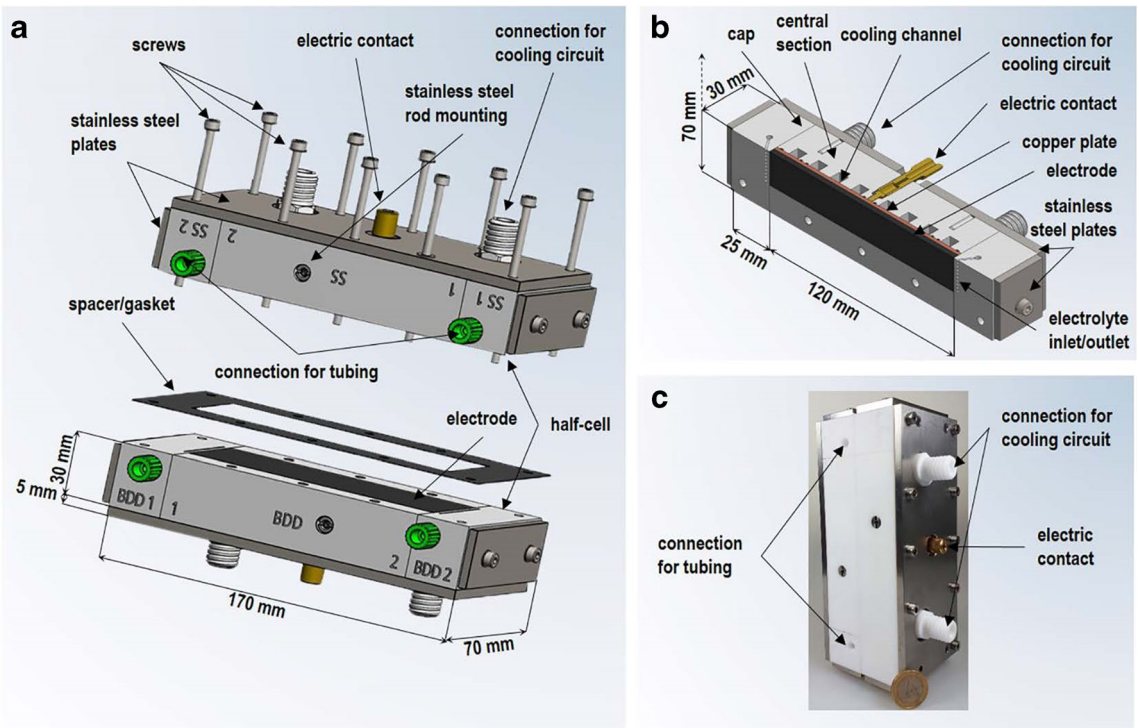

Fig. 7 Technical drawings of 4 cm × 12 cm flow electrolysis cell. **a** Partly exploded drawing of the full-featured flow cell. **b** Cross-section of one half-cell. **c** Completely mounted 4 cm × 12 cm flow electrolysis cell and a Euro coin (diameter: 23.25 mm) for comparison. Reprinted with permission [107]. Copyright [2020] American Chemical Society

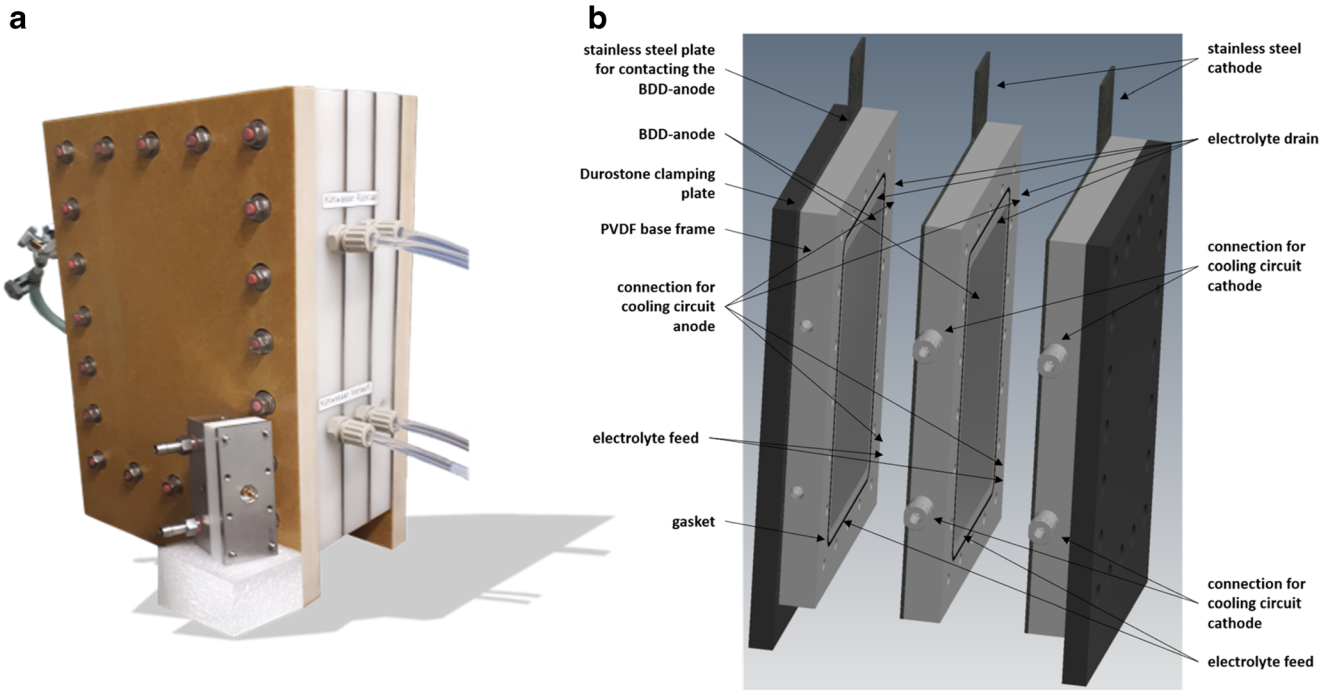

Fig. 8 EUT pilot cell: **a** EUT pilot cell with 2 cm × 6 cm flow electrolysis cell for size comparison. **b** Technical drawing of three Polyvinylidene fluoride (PVDF) frames with inserted BDD electrodes, cooling connections, electrolyte feed and gaskets

to the increased electrode surface area. With these settings, **5** could be obtained in the form of a ten-step cascade with an isolated yield of 49% (Table 4, Entry 1).

However, the electrolysis process generated a lot of heat, which is why the cell was cooled to 0 °C for the next electrolysis. This led to a slightly lower warming and also a slightly higher isolated yield of 51% (Table 4, Entry 2). As a result, the supporting electrolyte quantity was successively reduced. First to 0.010 mol/L, which gave an isolated yield of 56% (Table 4, Entry 3). Then to 0.005 mol/L, the value that was optimal for electrolysis on a smaller scale. This second lowering of the supporting electrolyte concentration resulted in an isolated yield of 59% (Table 4, Entry 4). Thus, the electrochemical synthesis of **5** was successfully transferred to technical scale without any loss of yield (Table 6, Entry 4). The conditions previously optimized on a small laboratory scale were largely retained, which is a confirmation of the optimization and scaling-up methodology used. A EUT pilot cell with glassy carbon electrodes was not available. Therefore, pyridine as additive was not tested jet, because this system works best with glassy carbon electrodes [83].

Other strategies for effective removal of hydrogen from the flow electrolysis cell

Electrolysis often leads to gas development as a counter-reaction. Thus, hydrogen is produced at the cathode by reduction of protons, while oxygen is usually formed at the anode. In beaker-type electrolysis cells of a batch process, this is generally not a problem, as the gas can escape freely upwards out of the cell. Whereas in a flow electrolysis process, the gas development can become a challenge, which is due to the special

Table 4 Optimization of the electrochemical synthesis of **5** using the EUT pilot cell

Entry	c($MeBu_3NO_3SOMe$) [$\frac{mol}{L}$]	j [$\frac{mA}{cm^2}$]	T [°C]	ν [$\frac{mL}{min}$]	Yield **5**
1	0.020	40	10	38.8	49%
2	0.020	40	0	38.8	51%
3	0.010	40	0	38.8	56%
4	0.005	40	0	38.8	59%
5	0.005	40	−10	38.8	58%

Electrolysis conditions: 2.0 mol/L 2,4-dimethylphenol (**4**), HFIP, BDD||stainless steel, anode area: 312 cm^2 applied charge: 10 × 0.1 F, interelectrode gap: 0.025 cm. Number of cascade steps: 10. j: current density. T: temperature. ν: flow rate. Isolated yield

geometry of a flow electrolysis cell. Flow electrolysis cells are usually closed systems, except for an electrolyte inlet and outlet. In the case of flow electrolysis cells with a very small electrode gap ("narrow gap"), as used in this work, the cell volume is also very small. In such cases, the gas produced during electrolysis cannot simply escape from the cell but takes up a non-negligible part of the cell volume, which disturbs the course of the electrolysis. This effect increases from bottom to top if the cell is vertically oriented, since firstly, more and more gas bubbles are formed on the way to the cell outlet and secondly, these bubbles combine to form larger gas bubbles (Fig. 9).

Since the cell volume is occupied by hydrogen gas (bubbles), the actual current density no longer corresponds to the theoretically calculated one. This is because the electrode surface is no longer completely covered with electrolyte. In addition, the terminal voltage increases and fluctuates very strongly. Finally, the dwell time of the electrolyte in the cell becomes uncontrollable. As a result, the reproducibility decreases. One way to address this problem is to pump the electrolyte through the cell faster. This also means that the resulting gas bubbles are expelled from the cell more quickly and can therefore no longer combine so easily to form large gas bubbles, nor do they take up so much cell volume. This strategy has already been successfully implemented by means of cascade electrolysis.

In addition, a strategy was developed in which the gas is directly separated during electrolysis. The homocoupling of **4** to **5** described here was chosen as an example reaction, in which hydrogen is produced at the cathode as a counter reaction. To realize a separation of the cathodically produced hydrogen during electrolysis in the narrow gap flow electrolysis cell, perforated stainless steel sheets were used as cathodes (Fig. 10). The holes in the cathode should allow the hydrogen to escape directly from the cell into the environment during electrolysis.

Various perforations were examined: Wide longitudinal slits running lengthwise over the entire electrode surface and should be able to discharge a large amount of hydrogen as effectively as possible (perforated stainless steel plate B). The triangular shape of the slits of perforated stainless steel sheet C, which becomes wider towards the top, is intended on the one hand to prevent excessive leakage of electrolyte via the openings of the electrode, and on the other hand the special shape is adapted to the process of hydrogen evolution: At the beginning, rather few and small hydrogen bubbles are formed, whereas there are rather many large bubbles at the end of the cell. Variant D is a plate with many small round holes, which are homogeneously distributed over the entire electrode surface, and perforated stainless steel plate E is designed to function like perforated stainless steel plate B. However, the slits are located orthogonally to the direction of flow, this is also intended to prevent the electrolyte from being excessively distributed outside the cell volume. The individual electrodes were mounted on a Teflon block specially developed for this application, which has a cavity lined with stainless steel (for contacting reasons) on the electrode side (Fig. 11).

The formed hydrogen is collected in this cavity and then exits through two small openings on the back of the cell. This Teflon block can be modularly connected to the 2 cm × 6 cm flow electrolysis cell. It is also important that the flow electrolysis cell in this system is operated horizontally with the

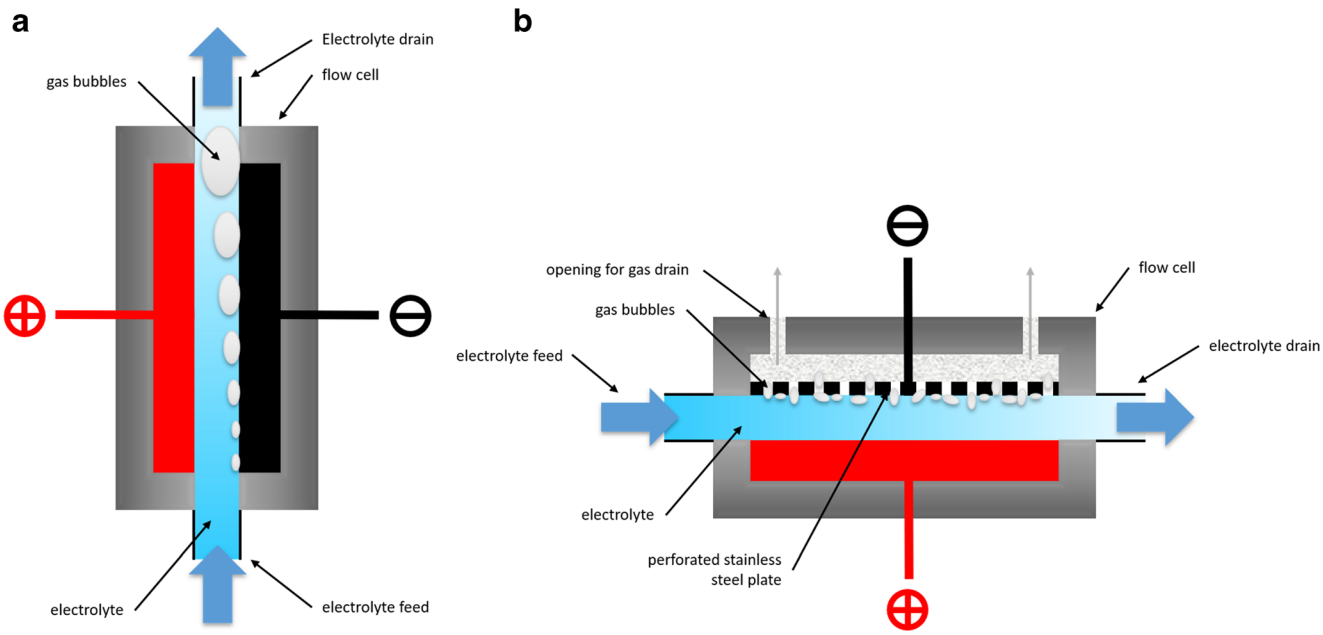

Fig. 9 **a** Schematic illustration of the hydrogen gas evolution in a vertically operated flow electrolysis cell. **b** Schematic illustration of the hydrogen gas discharge in a horizontally operated flow electrolysis cell with perforated stainless steel plates used as cathode

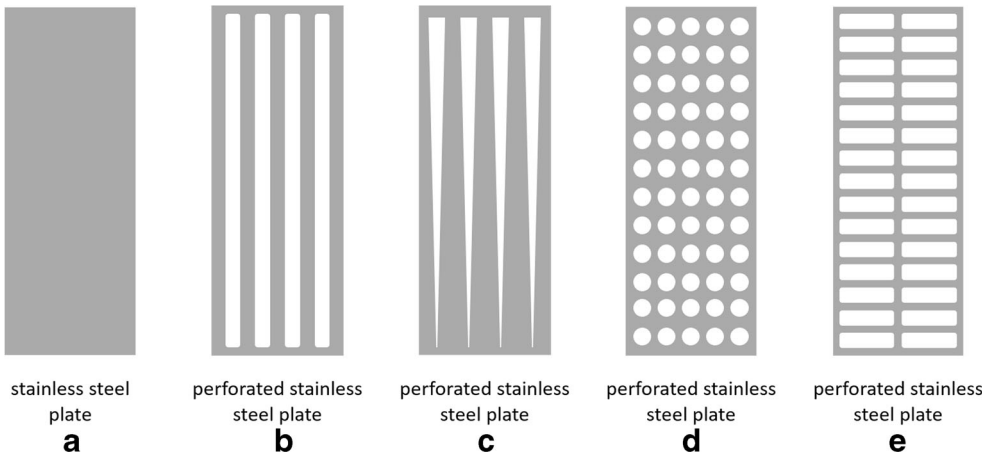

Fig. 10 Selection of different cathode geometries. **a** Conventional plate electrode. **b**–**e** Differently perforated stainless steel plates for direct hydrogen separation

cathode side facing upwards so that the hydrogen can easily escape upwards and prevents the electrolyte from running out of the flow electrolysis cell. Up to now, the flow electrolysis cell has always been operated vertically, as this ensures a constant flow rate and allows the hydrogen to escape upwards. To have a reference for horizontal electrode alignment, an electrolysis was first carried out with a classical plate electrode as cathode in horizontal alignment. This allowed an isolated yield of 31% of **5** (Fig. 12, A). The yield is relatively low, which can be explained by the fact that the optimized conditions were not used for test purposes and no cascade electrolysis was performed (electrolysis conditions: see Fig. 12). In addition, the horizontal operation of the cell leads to the hydrogen collecting at the top of the cathode (which is intentional in the case of perforated cathodes), thus preventing undisturbed electrolysis. In addition, the electrolyte does not run out of the cell continuously, but rather in an oscillating way: The electrolyte first accumulates in the cell until a certain level is reached. Then this electrolyte suddenly runs out of the cell. A constant setting of the flow rate is not possible in this way.

The use of the perforated cathodes B – C (Fig. 11), should now change this behavior in the way that the hydrogen can escape upwards and the electrolyte can flow out of the cell in a gas-free and controlled manner. The resulting isolated yields of **5** are actually higher than the yield when using a simple stainless steel plate as the cathode, with values of 33% for stainless steel perforated plate C and 41% for stainless steel perforated plate D (Fig. 12). However, the problem of intermittent electrolyte outflow could not be solved. On the contrary, the additional openings of the flow electrolysis cell, which were intended for hydrogen removal, drew more air into the cell than was the case with the non-perforated plate electrode. Hydrogen separation was therefore not possible. Even higher flow rates did not lead to an improvement, but rather to that the electrolyte escaping at the additional openings of the cathode.

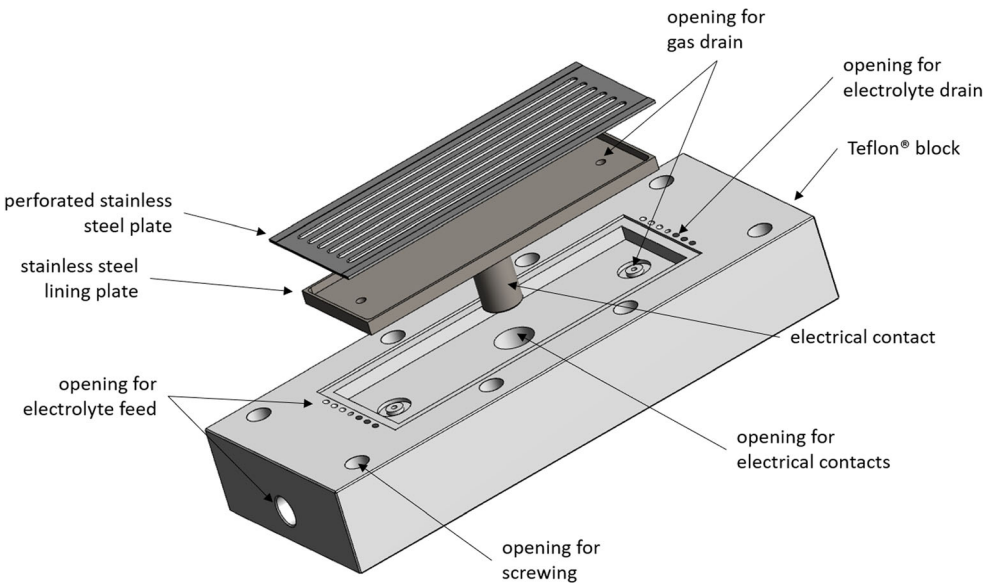

Fig. 11 Cathodic side of a 2 cm × 6 cm flow electrolysis cell for the use of perforated stainless steel plates

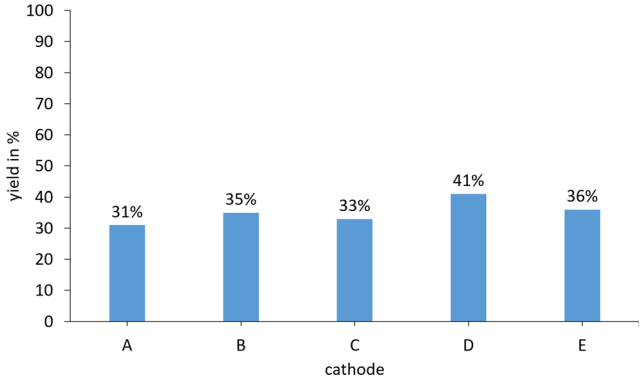

Fig. 12 Isolated yield of **5** using different cathode geometries (see Fig. 11). Electrolysis conditions: 1.0 mol/L 2,4-dimethylphenol (**4**), 0.01 mol/L $MeBu_3NO_3SOMe$, HFIP, BDD||stainless steel, anode area: 12 cm^2, current density: 20 mA/cm^2, applied charge: 1.0*F*, flow rate: 0.15 mL/min, interelectrode gap: 0.05 cm, 22 °C, Mode: single step, horizontal arrangement of the cell

Since these attempts at hydrogen separation were not successful, the idea of perforated plates was rejected, and a different strategy was pursued. Instead of a planar arrangement from cathode to anode, a cell was built in which the cathode (stainless steel plate electrode) was inserted into the Teflon® block obliquely (Fig. 13).

Thus, the cell volume increases over the length of the flow electrolysis cell. The volume of the evolved hydrogen is increasing inside the cell on the way from the electrolyte inlet to the outlet. Due to the inclined electrode arrangement of the cathode, the hydrogen has more available space. This leads to a less interruption of the electrolysis by gas bubbles. In addition, there is an opening at the top of each of the two sides of the electrolysis cell through which the hydrogen can escape. To test the function of this new cell, it was operated in four different modes: In horizontal and vertical alignment, one with open and one with closed openings for the hydrogen. The results of these tests are shown in Table 5.

In general, the isolated yields are comparable with the reference electrolysis (vertically performed electrolysis with parallel electrode arrangement). Accordingly, there is no decrease in isolated yield due to the changed electrode arrangement. With the two closed variants, no gas separation occurs, and electrolyte and hydrogen are discharged from the electrolyte outlet. But also, in the vertically open variant the hydrogen could not be separated. However, the stable isolated yields, coupled with low voltage fluctuations during electrolysis, indicate that the electrolysis is less disturbed by hydrogen evolution and therefore gains in reproducibility. A partially functioning gas separation could be realized with horizontal open operation. Here, however, gas-free discharge of the electrolyte and air intake through the lateral openings alternated.

In summary, none of the investigated cathode systems was completely convincing and effectively contributed to gas separation and a significant improvement in electrolysis performance. Open systems, which are necessary for hydrogen separation, tend to lead to new problems of a hydrodynamic nature. The strategy of giving the resulting hydrogen more space on its way through the cell promises to be more successful. However, the cell tested here is only the beginning of development in this direction and will need to be further elaborated in the future.

Analysis of by-products occurring during the electrolysis of 4

In addition to the desired dehydrogenative homocoupling of **4** to **5** as the main product, by-product formation also occurs, mainly through over-oxidation. To get an idea of which by-products can occur during the electrolysis of **5** in the system developed here, the individual signals of a gas chromatogram were assigned to the by-products with the help of authentic substances and GC-MS (Fig. 14).

First, it is noticeable that many different by-products are formed. However, it must be said that the proportion of by-products visible here is very small compared to the product **5**. This becomes especially clear when aware that for this sample much of **5** has already been removed from the mixture before the GC was measured, to record as many by-

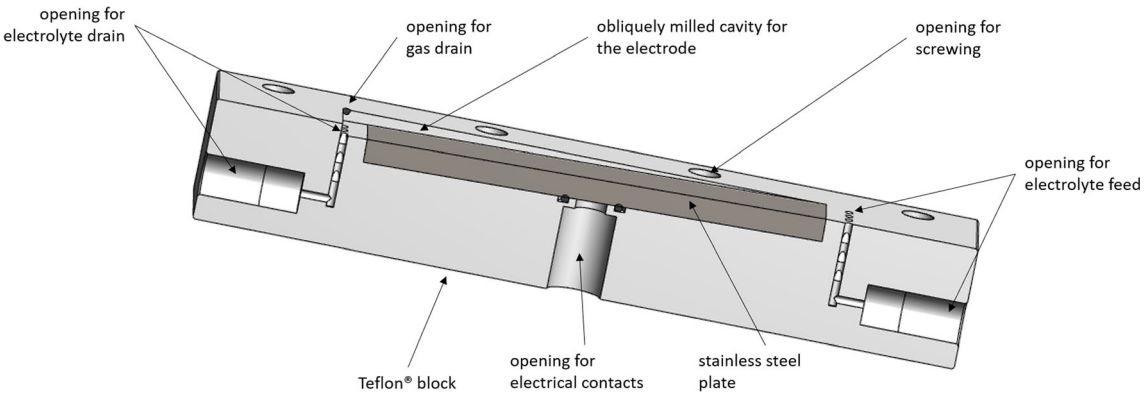

Fig. 13 Cross-section of the cathode side of a 2 cm × 6 cm flow electrolysis cell with inclined stainless steel plate electrode

Table 5 Screening of different operating modes with inclined cathode arrangement in the 2 cm × 6 cm flow electrolysis cell

Entry	Operation mode	Openings	Yield **5**
1	vertical	open	33%
2	vertical	closed	32%
3	horizontal	open	31%
4	horizontal	closed	32%
5	Reference (co-planar)	closed	30%

Electrolysis conditions: 1.0 mol/L 2,4-dimethylphenol (**4**), 0.01 mol/L $MeBu_3NO_3SOMe$, HFIP, BDD||stainless steel, anode area: 12 cm^2, current density: 20 mA/cm^2, applied charge: 1.0*F*, flow rate: 0.15 mL/min, interelectrode gap: 0.05 cm, 22 °C. Mode: single step, horizontal or vertical arrangement of the cell. Isolated yield

products as possible. The electrosynthesis is therefore still very selective.

The occurring by-products can be divided into three classes. First, there are brominated by-products, such as 2-bromo-4,6-dimethylphenol (Fig. 14, red) and a brominated derivative of **5** (Fig. 14, pink). These are only formed when NEt_4Br (or other brominated salts) are used as supporting electrolyte. The second class are polycyclic compounds: A derivative of the *Pummerer* ketone (Fig. 14, dark red), a spirolactone (Fig. 14, orange) and a pentacyclic compound (Fig. 14, purple). Although this group of by-products is mainly formed under basic conditions [61–65] to a smaller extent it is also formed in the electrolyte system used here. The third class are linear coupling products of **4**, including the diphenyl ether of **4** (Fig. 14, petrol), the ortho-meta coupling product (Fig. 14, pink) or higher coupling products such as the dehydrotrimer (Fig. 14, dark green). As can be seen from the relatively large signal for the dehydro trimer, this is the predominant side reaction path under acidic to neutral conditions, such as those prevailing in HFIP [61, 70, 71, 76]. The process of over-oxidation starting from the dehydro trimer can go even further and thus oligomeric or even polymeric over-oxidation products can be formed. This reaction path was confirmed by an APCI-MS measurement (Supporting information).

Conclusion

In summary, the electrochemical synthesis of 3,3′,5,5’-tetramethyl-2,2′-biphenol (**5**) has been successfully scaled-up from the laboratory scale to a continuous technical scale. For this scale-up with immediate optimization of the reaction parameters, modular narrow gap electrochemical flow cells were developed in the Waldvogel group. Thus, a stepwise scale-up was successfully achieved. Using the same cell geometry in all three sizes of flow cells, the electrolysis conditions can almost be transferred and all three differently sized elecrolysis ellsc the desired product **5** can be obtained in a yield of app. 60% (Table 6). However, the EUT pilot cell developed for the technical scale must be optimized regarding a more effective heat dissipation to allow a smooth continuous operation of the electrolysis cell. Furthermore, the resulting gaseous hydrogen can be efficiently transported out of the flow cell by an increased flow rate in the cascade mode. Nevertheless, we will continue to investigate the cell type and the emerging challenges such as hydrogen evolution and heat dissipation.

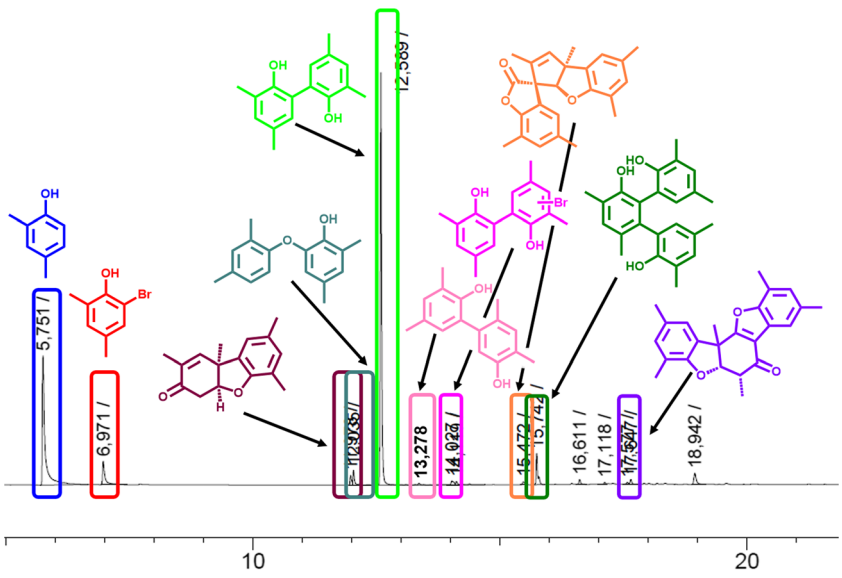

Fig. 14 Segment of a gas chromatogram of the residue obtained after the work-up of the electrolysis mixture upon removal of most **5** since otherwise the by-products are difficult so see. The signals are signed to the individual by-products

Table 6 Comparison of optimized conditions for different electrolysis cells

Entry	Cell-type	Solvent	c(Supporting electrolyte) $[\frac{mol}{L}]$	Q [*F*]	j $[\frac{mA}{cm^2}]$	T [°C]	Electrode material	ν $[\frac{mL}{min}]$	Yield **5**	Productivity $[\frac{g}{min}]$
1	Batch (25 mL)	HFIP +15 vol.% H_2O	Et_4NBr 0.08	1.2	6.1	50	GC||GC	–	46%	0.002
2	2 × 6 Flow	HFIP	$MeBu_3NO_3SOMe$ 0.005	1.0 (10 × 0.1)	60	10	BDD||SS	2.24	62%	0.3
3	4 × 12 Flow	HFIP	$MeBu_3NO_3SOMe$ 0.005	1.0 (10 × 0.1)	60	10	BDD||SS	8.95	58%	1.3
4	EUT Pilot cell	HFIP	$MeBu_3NO_3SOMe$ 0.005	1.0 (10 × 0.1)	40	0	BDD||SS	38.8	59%	16.9

Electrolysis conditions: 2.0 mol/L 2,4-dimethylphenol (**4**), for all flow cells: interelectrode gap d: 0.025 cm. Q: applied charge. j: current density. T: temperature. ν: flow rate. GC: glassy carbon. BDD: boron-doped diamond. SS: stainless steel. Isolated Yields

Experimental

General information

All reagents were used in analytical grade. Solvents were purified by standard methods [108]. As supporting electrolyte *N*-methyl-*N*,*N*,*N*-tributylammonium methylsulfate (kindly provided by BASF SE, Ludwigshafen, Germany) were used.

Electrode materials For electrochemical reactions boron-doped diamond (BDD, 15 μm diamond layer on silicon, DIACHEM™, obtained from CONDIAS, Itzehoe, Germany) and glassy carbon (SIGRADUR G, obtained from HTW Hochtempatur Werkstoffe GmbH, Thierhaupten, Germany) were applied as electrode material.

Power supplies As a power supply for the 2 cm × 6 cm flow cell, a self-built one-channel galvanostat (dc output 0–70 V and 0–1 A) with a self-built Coulomb counter of University Bonn were used. For the 4 cm × 12 cm flow cell, a TDK Lamda Z60–3.5 power supply (dc output 0–60 V and 0–3.5 A, rated power 210 W; TDK Lambda, Achern, Germany) was applied. For the EUT Pilot cell, a TDK Lamda G150–34 power supply (dc output 0–150 V and 0–34 A, rated power 5 kW; TDK Lambda, Achern, Germany) was applied. The electric current was adjusted for the given current density, whereas the voltage was set freely.

Pumps For pumping the electrolytes through the 2 cm × 6 cm flow cell, an Ismatec Reglo ICC Digital Peristaltic Pump MS-2/12 (2 Channels, 12 pump rollers, flow rate: 0.002–38 ml/min per channel; Cole-Parmer GmbH, Wertheim, Germany) with a PharMed® BPT tubing (ID: 0.25 mm, wall: 0.90 mm and ID: 2.06 mm, wall: 0.91 mm); IDES Health & Science GmbH, Wertheim, Germany) were used. For pumping the electrolytes through the 4 cm × 12 cm flow cell, a Fink Ritmo R033/7–16 pump (Stroke volume: 0.74 mL, max. Stroke frequency: 190 strokes/min, max. Pressure: 16 bar, flow rate: 0.0417–125 mL/min; Fink Chem + Tec GmbH, Leinfelden-Echterdingen, Germany) were used. For pumping the electrolytes through the EUT Pilot cell, two Fink Ritmo R05/120 pumps (Stroke volume: 2.65 mL, max. Stroke frequency: 46 strokes/min, max. Pressure: 2 bar, flow rate: 0.12–120 mL/min; Fink Chem + Tec GmbH, Leinfelden-Echterdingen, Germany) were used.

Temperature control For external temperature control, a Julabo F33-MA refrigerated circulator (working temperature: –30 °C – 200 °C, heating power: 2 kW, cooling power (ethanol): 0.5 kW (20 °C), 0.32 kW (0 °C), 0.12 kW (−20 °C), 0.03 kW (−30 °C), flow rate: 11–16 L/min; Julabo GmbH, Seelbach, Germany) was used.

Column chromatography A preparative chromatography system Sepacore® Flash System X10/X50 (Büchi Labortechnik AG, Flawil, Switzerland) with a Büchi control unit C-620, a UV detector Büchi UV Photometer C-635, Büchi fraction collector C-660 and two pump modules C-605 for adjusting the solvent mixture were used for column chromatographic purification together with a 90 g disposable polypropylene cartridge filled with silica gel 60 M (0.060–0.200 mm, Macherey-Nagel GmbH & Co., Düren, Germany). As eluent a mixture of cyclohexane (solvent A) and ethyl acetate (solvent B) was used, both purified in the rotary evaporator. The following gradient was run at a flow rate of 75 mL/min and a maximum pressure of 10 bar. 12 min 0 s, 0% solvent B; 20 min 5 s, 0–1% solvent B; 15 min 0 s, 1–2% solvent B; 12 min 5 s, 2–4% solvent B; 5 min 5 s, 4–8% solvent B; 5 min 5 s, 8–16% solvent B; 5 min 5 s, 16–32% solvent B; 5 min 5 s, 32–100% solvent B; 5 min 0 s, 100% solvent B. Silica gel 60 plates on aluminum (F254, Merck, Darmstadt, Germany) were used for thin layer chromatography.

Analysis ^{1}H and ^{13}C NMR spectra were recorded at 25 °C by using a Bruker Avance III HD 400 (Bruker, Germany). Chemical shifts (δ) are reported in parts per million (ppm) relative to tetramethylsilane as internal standard or traces of $CHCl_3$ in the corresponding deuterated solvent. Gas chromatography was performed on a Shimadzu GC-2010 (Shimadzu, Japan) using a ZB-5 column (Phenomenex, USA; length: 30 m, inner diameter: 0.25 mm, film: 0.25 mm, carrier gas: hydrogen).

Synthesis of 3,3′,5,5′-tetramethyl-2,2′-biphenol (5)

A solution of 2,4-dimethylphenol (**4**) and the corresponding supporting electrolyte were dissolved in HFIP and if used the appropriate additive. The solution was pumped through the electrochemical flow cell. The corresponding electrochemical parameters were applied during the electrolysis. After electrolysis, the solvent mixture was almost completely recovered at reduced pressure (200 mbar, 50 °C), just until crystallization of the product occurs. To complete the crystallization, the mixture was placed in the fridge (8 °C) overnight. The product was filtered off by suction and washed with cyclohexane and dried overnight in high vacuum ($1{\cdot}10^{-3}$ mbar, 20 °C). The mother liquor contains the supporting electrolyte and still some product (**5**). The solvent of the mother liquor was removed in vacuo (50 °C, 200–20 mbar) and the residue was dissolved in ethyl acetate and washed three times by distilled water. The organic fractions were united and washed one time with ethyl acetate. Afterwards the united aqueous phase was completely evaporated in vacuo (50 °C, 70–10 mbar) and dried in vacuum ($1{\cdot}10^{-3}$ mbar, 20 °C) to obtain the supporting electrolyte. The organic phase was washed with brine, dried over $MgSO_4$ and the solvent is removed at reduced pressure (50 °C, 200–10 mbar). The residue was distilled in vacuum (15 mbar – 20 mbar, 95 °C) to obtain leftover starting material (**4**). The remaining residue was boiled three times for 1 h in *n*-heptane. After cooling down, the residue was decanted. The three extracts of *n*-heptane were united and the solvent was removed under pressure (50 °C, 200–20 mbar) just until crystallization of the product occurs. After 1 h cooling in the fridge (8 °C) to complete crystallization. The product was filtered off by suction and washed with cyclohexane and drying in vacuum ($1{\cdot}10^{-3}$ mbar, 20 °C) obtain further product (**5**). The analytical data were in accordance with those reported in literature [83]. Details of the synthesis in every type of electrochemical flow cell and the corresponding electrolysis conditions are listed in the supporting information.

Supplementary Information The online version contains supplementary material available at https://doi.org/10.1007/s41981-020-00121-6.

Acknowledgements Open Access funding enabled and organized by Projekt DEAL.

Authors contributions Not applicable.

Funding This work was funded by the Federal Ministry of Education and Research Project EPSYLON (FKZ 13XP5016D). In addition, financial support by the DFG (Wa1276/24–1) is highly appreciated. The financial support by the Graduate School Materials Science in Mainz (GSC 266) is greatly acknowledged.

Data availability Supporting information, which contains technical drawings and pictures of the flow cells used. Furthermore, optimization experiments and detailed data are found here.

Compliance with ethical standards

Conflicts of interest/ competing interests The authors declare no conflict of interest and competing financial interests.

Code availability Not applicable.

References

1. Bringmann G, Gulder T, Gulder TAM, Breuning M (2011) Atroposelective total synthesis of axially chiral biaryl natural products. Chem Rev 111(2):563–639

2. von Nussbaum F, Brands M, Hinzen B, Weigand S, Häbich D (2006) Antibacterial natural products in medicinal chemistry – exodus or revival? Angew Chem Int Ed 45(31):5072–5129
3. Ogura T, Usuki T (2013) Total synthesis of acerogenins E, G and K, and centrolobol. Tetrahedron 69(13):2807–2815
4. Lee Y-J, Lee YM, Lee C-K, Jung JK, Han SB, Hong JT (2011) Therapeutic applications of compounds in the Magnolia family. Pharmacol Ther 130(2):157–176
5. Patočka J, Jakl J, Strunecká A (2006) Expectations of biologically active compounds of the genus Magnolia in biomedicine. J Appl Biomed 4(4):171–178
6. Satomi H, Umemura K, Ueno A, Hatano T, Okuda T, Noro T (1993) Carbonic anhydrase inhibitors from the pericarps of Punica Granatum L. Biol Pharm Bull 16(8):787–790
7. Losey HC, Peczuh MW, Chen Z, Eggert US, Dong SD, Pelczer I, Kahne D, Walsh CT (2001) Tandem action of glycosyltransferases in the maturation of vancomycin and teicoplanin aglycones: novel glycopeptides. Biochemistry 40(15):4745–4755
8. Williams DH, Bardsley B (1999) The vancomycin group of antibiotics and the fight against resistant bacteria. Angew Chem Int Ed 38(9):1172–1193
9. Bringmann G, Price Mortimer AJ, Keller PA, Gresser MJ, Garner J, Breuning M (2005) Atroposelective synthesis of axially chiral biaryl compounds. Angew Chem Int Ed 44(34):5384–5427
10. Alexakis A, Polet D, Rosset S, March S (2004) Biphenol-based phosphoramidite ligands for the enantioselective copper-catalyzed conjugate addition of diethylzinc. J Org Chem 69(17):5660–5667
11. Brunel JM (2005) BINOL: a versatile chiral reagent. Chem Rev 105(3):857–897
12. Alexakis A, Polet D, Benhaim C, Rosset S (2004) Biphenol-based ligands for cu-catalyzed asymmetric conjugate addition. Tetrahedron Asymmetry 15(14):2199–2203
13. d'Augustin M, Palais L, Alexakis A (2005) Enantioselective copper-catalyzed conjugate addition to trisubstituted cyclohexenones: construction of stereogenic quaternary centers. Angew Chem Int Ed 44(9):1376–1378
14. Vuagnoux-d'Augustin M, Alexakis A (2007) Copper-catalyzed asymmetric conjugate addition of trialkylaluminium reagents to trisubstituted enones: construction of chiral quaternary centers. Chem Eur J 13(34):9647–9662
15. Pang Z, Xing A, Wang L (2015) Synthesis of novel tartaric acid-derived chiral phosphite ligands and their application in the cu-catalyzed conjugate addition of diethylzinc to cyclic enones. Chem Res Chin Univ 31(5):756–760
16. Monti C, Gennari C, Piarulli U (2005) Enantioselective conjugate addition of phenylboronic acid to enones catalysed by a chiral tropos/atropos rhodium complex at the coalescence temperature. Chem Commun (42):5281–5283
17. Monti C, Gennari C, Piarulli U (2007) Rh-catalyzed enantioselective conjugate addition of arylboronic acids with a dynamic library of chiral tropos phosphorus ligands. Chem Eur J 13(5):1547–1558
18. Monti C, Gennari C, Piarulli U, de Vries JG, de Vries AHM, Lefort L (2005) Rh-Ratalyzed asymmetric hydrogenation of prochiral olefins with a dynamic library of chiral TROPOS phosphorus ligands. Chem Eur J 11(22):6701–6717
19. Mata Y, Pàmies O, Diéguez M (2007) Screening of a modular sugar-based phosphite-oxazoline ligand library in asymmetric Pd-catalyzed heck reactions. Chem Eur J 13(12):3296–3304
20. Raluy E, Diéguez M, Pàmies O (2007) Sugar-based diphosphoroamidite as a promising new class of ligands in Pd-catalyzed asymmetric allylic alkylation reactions. J Org Chem 72(8):2842–2850
21. Franke R, Selent D, Börner A (2012) Applied hydroformylation. Chem Rev 112(11):5675–5732
22. Mormul J, Mulzer M, Rosendahl T, Rominger F, Limbach M, Hofmann P (2015) Synthesis of adipic aldehyde by n-selective hydroformylation of 4-Pentenal. Organometallics 34(16):4102–4108
23. Smith SE, Rosendahl T, Hofmann P (2011) Toward the rhodium-catalyzed bis-hydroformylation of 1,3-butadiene to adipic aldehyde. Organometallics 30(13):3643–3651
24. Gütz C, Stenglein A, Waldvogel SR (2017) Highlymodular flow cell for electroorganic synthesis. Org Process Res Dev 21(5):771–778
25. Bamberger E, Brun J (1907) Über die Einwirkung Alkoholischer Schwefelsäure auf 2.4-Dimethyl-chinol. Ber Dtsch Chem Ges 40(2):1949–1955
26. Cosgrove SL, Waters WA (1951) The oxidation of phenols with the free hydroxyl radical. J Chem Soc 1726–1730. https://doi.org/10.1039/JR9510001726
27. Baddiley J, Buchanan JG, Handschumacher RE, Prescott JF (1956) Chemical studies in the biosynthesis of purine nucleotides. Part I. The preparation of N-glycylglycosylamines. J Chem Soc 2818–2823. https://doi.org/10.1039/JR9560002818
28. Kaeding WW (1963) Oxidation of phenols with cupric salts. J Org Chem 28(4):1063–1067
29. Elovitz MS, Fish W (1995) Redox interactions of Cr(VI) and substituted phenols: products and mechanism. Environ Sci Technol 29(8):1933–1943
30. Barrett AGM, Itoh T, Wallace EM (1993) (η6-benzene)(η5-ethyltetramethylcyclopentadienyl)rhodium (III) hexafluorophosphate: a reagent for catalytic phenol oxidative coupling. Tetrahedron Lett 34(14):2233–2234
31. Hwang D-R, Chen C-P, Uang B-J (1999) Aerobic catalytic oxidative coupling of 2-naphthols and phenols by VO(acac)2. Chem Commun (13):1207–1208
32. Yadav JS, Reddy BVS, Uma Gayathri K, Prasad AR (2003) [Bmim]PF6/RuCl3·xH2O: a novel and recyclable catalytic system for the oxidative coupling of β-naphthols. New J Chem 27(12):1684–1686
33. Sharma VB, Jain SL, Sain B (2003) Methyltrioxorhenium-catalyzed aerobic oxidative coupling of 2-naphthols to binaphthols. Tetrahedron Lett 44(13):2655–2656
34. Jiang Q, Sheng W, Tian M, Tang J, Guo C (2013) Cobalt(II)-Porphyrin-catalyzed aerobic oxidation: oxidative coupling of phenol. Eur J Org Chem 10:1861–1866. https://doi.org/10.1002/ejoc.201201595
35. International Resource Panel of the United Nations Environmental Programme (2017) Assessing global resource use: a systems approach to resource efficiency and pollution reduction. UNESCO, Nairobi
36. IPCC (2013) Summary for Policymakers. In: Climate Change 2013: the physical science basis. Contribution of Working Group I to the Fifth Assessment Report of the Intergovernmental Panel on Climate Change. Cambridge University Press, Cambridge, United Kingdom and New York, NY, USA
37. IPCC (2015) Climate change 2014: synthesis report. Contribution of working groups I, II and III to the Fifth Assessment Report of the Intergovernmental Panel on Climate Change. IPCC, Geneva, Switzerland
38. Olivier JGJ, Janssens-Maenhout G, Muntean M (2016) Trends in global CO2 emissions: 2016 report, The Hague
39. Lin D, Hanscom L, Murthy A, Galli A, Evans M, Neill E, Mancini M, Martindill J, Medouar F-Z, Huang S, Wackernagel M (2018) Ecological footprint accounting for countries: updates and results of the National Footprint Accounts, 2012–2018. Resources 7:58–80
40. REN21 (2019) Renewables 2019. Global Status Report. REN21 Secretariat, Paris
41. Anastas P, Eghbali N (2010) Green chemistry: principles and practice. Chem Soc Rev 39(1):301–312

42. Steckhan E, Arns T, Heineman WR, Hilt G, Hoormann D, Jörissen J, Kröner L, Lewall B, Pütter H (2001) Environmental protection and economization of resources by electroorganic and electroenzymatic syntheses. Chemosphere 43(1):63–73
43. Frontana-Uribe BA, Little RD, Ibanez JG, Palma A, Vasquez-Medrano R (2010) Organic electrosynthesis: a promising green methodology in organic chemistry. Green Chem 12(12):2099–2119
44. Schäfer HJ (2011) Contributions of organic electrosynthesis to green chemistry. C R Chimie 14(7–8):745–765
45. Elsherbini M, Wirth T (2019) Electroorganic synthesis under flow conditions. Acc Chem Res 52(12):3287–3296
46. Noël T, Cao Y, Laudadio G (2019) The fundamentals behind the use of flow reactors in electrochemistry. Acc Chem Res 52(10):2858–2869
47. Lund PD, Lindgren J, Mikkola J, Salpakari J (2015) Review of energy system flexibility measures to enable high levels of variable renewable electricity. Renew Sustain Energy Rev 45:785–807
48. Waldvogel SR, Lips S, Selt M, Riehl B, Kampf CJ (2018) Electrochemical arylation reaction. Chem Rev 118(14):6706–6765
49. Horn EJ, Rosen BR, Baran PS (2016) Synthetic organic electrochemistry: an enabling and innately sustainable method. ACS Cent Sci 2(5):302–308
50. Waldvogel SR, Janza B (2014) Renaissance of electrosynthetic methods for the construction of complex molecules. Angew Chem Int Ed 53(28):7122–7123
51. Shatskiy A, Lundberg H, Kärkäs MD (2019) Organic electrosynthesis: applications in complex molecule synthesis. ChemElectroChem 6(16):4067–4092
52. Sauermann N, Meyer TH, Qiu Y, Ackermann L (2018) Electrocatalytic C–H activation. ACS Catal 8(8):7086–7103
53. Yang Q-L, Fang P, Mei T-S (2018) Recent advances in organic electrochemical C-H functionalization. Chin J Chem 36(4):338–352
54. Yan M, Kawamata Y, Baran PS (2017) Synthetic organic electrochemical methods since 2000: on the verge of a renaissance. Chem Rev 117(21):13230–13319
55. Kärkäs MD (2018) Electrochemical strategies for C-H functionalization and C-N bond formation. Chem Soc Rev 47(15):5786–5865
56. Möhle S, Zirbes M, Rodrigo E, Gieshoff T, Wiebe A, Waldvogel SR (2018) Modern electrochemical aspects for the synthesis of value-added organic products. Angew Chem Int Ed 57(21):6018–6041
57. Wiebe A, Gieshoff T, Möhle S, Rodrigo E, Zirbes M, Waldvogel SR (2018) Electrifying organic synthesis. Angew Chem Int Ed 57(20):5594–5619
58. Röckl JL, Pollok D, Franke R, Waldvogel SR (2020) A decade of electrochemical dehydrogenative C,C-coupling of aryls. Acc Chem Res 53(1):45–61
59. Pollok D, Waldvogel SR (2020) Electro-organic synthesis – a 21st century technique. Chem Sci. https://doi.org/10.1039/D0SC01848A
60. Nilsson A, Ronlán A, Parker VD (1973) Anodic oxidation of phenolic compounds. Part III. Anodic hydroxylation of phenols. A simple general synthesis of 4-Alkyl-4-hydroxycyclo-hexa-2,5-dienones from 4-alkylphenols. J Chem Soc Perkin Trans 1(1973):2337–2345
61. Waldvogel SR (2010) Novel anodic concepts for the selective phenol coupling reaction. Pure Appl Chem 82(4):1055–1063
62. Barjau J, Schnakenburg G, Waldvogel SR (2011) Diversity-oriented synthesis of polycyclic scaffolds by modification of an anodic product derived from 2,4-dimethylphenol. Angew Chem Int Ed 50(6):1415–1419
63. Barjau J, Schnakenburg G, Waldvogel S (2011) Short domino sequence to Dioxa[4.3.3]propellanes. Synthesis 2011(13):2054–2061
64. Barjau J, Königs P, Kataeva O, Waldvogel S (2008) Reinvestigation of highly diastereoselective pentacyclic spirolactone formation by direct anodic oxidation of 2,4-Dimethylphenol. Synlett 15:2309–2312. https://doi.org/10.1055/s-2008-1078276
65. Malkowsky IM, Rommel CE, Wedeking K, Fröhlich R, Bergander K, Nieger M, Quaiser C, Griesbach U, Pütter H, Waldvogel SR (2006) Facile and highly diastereoselective formation of a novel pentacyclic scaffold by direct anodic oxidation of 2,4-Dimethylphenol. Eur J Org Chem (1):241–245
66. Malkowsky IM, Rommel CE, Fröhlich R, Griesbach U, Pütter H, Waldvogel SR (2006) Novel template-directed anodic phenol-coupling reaction. Chem Eur J 12(28):7482–7488
67. Rommel CE, Malkowsky I, Waldvogel SR, Puetter H, Griesbach U (2005) Anodic dimerization of substituted benzenes for the production of biarylalcohols. PCT Int Appl: WO 2005075709 A2 20050818
68. Malkowsky IM, Fröhlich R, Griesbach U, Pütter H, Waldvogel SR (2006) Facile and reliable synthesis of tetraphenoxyborates and their properties. Eur J Inorg Chem (8):1690–1697
69. Malkowsky IM, Griesbach U, Pütter H, Waldvogel SR (2006) Unexpected highly chemoselective anodicortho-coupling reaction of 2,4-dimethylphenol on boron-doped diamond electrodes. Eur J Org Chem 2006(20):4569–4572
70. Kirste A, Nieger M, Malkowsky IM, Stecker F, Fischer A, Waldvogel SR (2009) Ortho-selective phenol-coupling reaction by anodic treatment on boron-doped diamond electrode using fluorinated alcohols. Chem Eur J 15(10):2273–2277
71. Kirste A, Hayashi S, Schnakenburg G, Malkowsky IM, Stecker F, Fischer A, Fuchigami T, Waldvogel SR (2011) Highly selective electrosynthesis of biphenols on graphite electrodes in fluorinated media. Chem Eur J 17(50):14164–14169
72. Eberson L, Hartshorn MP, Persson O (1995) 1,1,1,3,3,3-Hexafluoropropan-2-ol as a solvent for the generation of highly persistent radical cations. J Chem Soc Perkin Trans 2(9):1735–1744
73. Eberson L, Hartshorn MP, Persson O, Radner F (1996) Making radical cations live longer. Chem. Commun (18):2105–2112
74. Colomer I, Chamberlain AER, Haughey MB, Donohoe TJ (2017) Hexafluoroisopropanol as a highly versatile solvent. Nat Rev Chem 1(11):88
75. Berkessel A, Adrio JA, Hüttenhain D, Neudörfl JM (2006) Unveiling the "booster effect" of fluorinated alcohol solvents: aggregation-induced conformational changes and cooperatively enhanced H-bonding. J Am Chem Soc 128(26):8421–8426
76. Kirste A, Schnakenburg G, Stecker F, Fischer A, Waldvogel SR (2010) Anodic phenol-arene cross-coupling reaction on boron-doped diamond electrodes. Angew Chem Int Ed 49(5):971–975
77. Francke R, Cericola D, Kötz R, Weingarth D, Waldvogel SR (2012) Novel electrolytes for electrochemical double layer capacitors based on 1,1,1,3,3,3-Hexafluoropropan-2-ol. Electrochim Acta 62:372–380
78. Waldvogel SR, Elsler B (2012) Electrochemical synthesis on boron-doped diamond. Electrochim Acta 82:434–443
79. Elsler B, Wiebe A, Schollmeyer D, Dyballa KM, Franke R, Waldvogel SR (2015) Source of selectivity in oxidative cross-coupling of aryls by solvent effect of 1,1,1,3,3,3-Hexafluoropropan-2-ol. Chem Eur J 21(35):12321–12325
80. Hollóczki O, Macchieraldo R, Gleede B, Waldvogel SR, Kirchner B (2019) Interfacial domain formation enhances electrochemical synthesis. J Phys Chem Lett 10(6):1192–1197
81. Hollóczki O, Berkessel A, Mars J, Mezger M, Wiebe A, Waldvogel SR, Kirchner B (2017) The catalytic effect of

fluoroalcohol mixtures depends on domain formation. ACS Catal 7(3):1846–1852
82. Selt M, Mentizi S, Schollmeyer D, Franke R, Waldvogel SR (2019) Selective and scalable dehydrogenative electrochemical synthesis of 3,3′,5,5′-Tetramethyl-2,2′-biphenol. Synlett 30(18): 2062–2067
83. Selt M, Franke R, Waldvogel SR (2020, in press) Supporting-electrolyte-free and scalable flow process for the electrochemical synthesis of 3,3′,5,5′-Tetramethyl-2,2′-biphenol. Org Process Res Dev. https://doi.org/10.1021/acs.oprd.0c00170
84. Arai T, Tateno H, Nakabayashi K, Kashiwagi T, Atobe M (2015) An anodic aromatic C,C cross-coupling reaction using parallel laminar flow mode in a flow microreactor. Chem Commun 51(23):4891–4894
85. Atobe M (2017) Organic electrosynthesis in flow microreactor. Curr Opin Electrochem 2(1):1–6
86. Horii D, Fuchigami T, Atobe M (2007) A new approach to anodic substitution reaction using parallel laminar flow in a micro-flow reactor. J Am Chem Soc 129(38):11692–11693
87. Horii D, Amemiya F, Fuchigami T, Atobe M (2008) A novel electrosynthetic system for anodic substitution reactions by using parallel laminar flow in a microflow reactor. Chem Eur J 14(33): 10382–10387
88. Kashiwagi T, Elsler B, Waldvogel SR, Fuchigami T, Atobe M (2013) Reaction condition screening by using electrochemical microreactor: application to anodic phenol-arene C,C Cross-coupling reaction in high acceptor number media. J Electrochem Soc 160(7):G3058–G3061
89. Elsherbini M, Winterson B, Alharbi H, Folgueiras-Amador AA, Génot C, Wirth T (2019) Continuous-flow electrochemical generator of hypervalent iodine reagents: synthetic applications. Angew Chem Int Ed 58(29):9811–9815
90. Folgueiras-Amador AA, Philipps K, Guilbaud S, Poelakker J, Wirth T (2017) An easy-to-machine electrochemical flow microreactor: efficient synthesis of isoindolinone and flow functionalization. Angew Chem Int Ed 56(48):15446–15450
91. Folgueiras-Amador AA, Qian X-Y, Xu H-C, Wirth T (2018) Catalyst- and supporting-electrolyte-free electrosynthesis of benzothiazoles and thiazolopyridines in continuous flow. Chem Eur J 24(2):487–491
92. Islam M, Kariuki BM, Shafiq Z, Wirth T, Ahmed N (2019) Efficient electrosynthesis of thiazolidin-2-imines via oxysulfurization of thiourea-tethered terminal alkenes using the flow microreactor. Eur J Org Chem 2019(6):1371–1376
93. Green RA, Brown RCD, Pletcher D (2016) Electrosynthesis in extended channel length microfluidic electrolysis cells. J. Flow Chem. 6(3):191–197
94. Green RA, Brown RCD, Pletcher D, Harji B (2015) A microflow electrolysis cell for laboratory synthesis on the multigram scale. Org Process Res Dev 19(10):1424–1427
95. Riehl B, Dyballa K, Franke R, Waldvogel S (2016) Electro-organic synthesis as a sustainable alternative for dehydrogenative cross-coupling of phenols and naphthols. Synthesis 49(02):252–259
96. Elsler B, Schollmeyer D, Dyballa KM, Franke R, Waldvogel SR (2014) Metal- and reagent-free highly selective anodic cross-coupling reaction of phenols. Angew Chem Int Ed 53(20):5210–5213
97. Wiebe A, Schollmeyer D, Dyballa KM, Franke R, Waldvogel SR (2016) Selective synthesis of partially protected nonsymmetric biphenols by reagent- and metal-free anodic cross-coupling reaction. Angew Chem Int Ed 55(39):11801–11805
98. Karthik PE, Alessandri I, Sengeni A (2020) A review on electrodes used in electroorganic synthesis and the significance of coupled electrocatalytic reactions. J Electrochem Soc 167(12): 125503
99. Cao Y, Soares C, Padoin N, Noël T (2021) Gas bubbles have controversial effects on Taylor flow electrochemistry. Chem Eng J 406:126811
100. Gieshoff T, Schollmeyer D, Waldvogel SR (2016) Access to pyrazolidin-3,5-diones through anodic N-N bond formation. Angew Chem Int Ed 55(32):9437–9440
101. Shih Y, Ke C, Pan C, Huang Y (2013) Transition-metal catalyst free C=N coupling with phenol/phenoxide: a green synthesis of a benzoxazole scaffold by an anodic oxidation reaction. RSC Adv 3(20):7330–7336
102. Salehzadeh H, Nematollahi D, Hesari H (2013) An efficient electrochemical method for the atom economical synthesis of some benzoxazole derivatives. Green Chem 15(9):2441–2446
103. Sharafi-Kolkeshvandi M, Nematollahi D, Nikpour F (2017) A regioselective and convergent paired electrochemical synthesis of N,N′-Diphenyl-3-sulfonyl-[1,1′-biphenyl]-4,4′-diamines. Synthesis 49(07):1555–1560
104. Pattison FLM, Stothers JB, Woolford RG (1956) Anodic syntheses involving w-monohalocarboxylic acids 1. J Am Chem Soc 78(10):2255–2259
105. Hammerich O, Speiser B (eds) (2016) Organic electrochemistry, fifth edition revised and expanded. CRC Press, Taylor & Francis Group, Boca Raton
106. Gleede B, Selt M, Gütz C, Stenglein A, Waldvogel SR (2019) Large, highly modular narrow-gap electrolytic flow cell and application in Dehydrogenative cross-coupling of phenols. Org Process Res Dev in press. https://doi.org/10.1021/acs.oprd.9b00451
107. Armarego WLF, Chai CLL (2013) Purification of laboratory chemicals7th edn. Elsevier, Amsterdam
108. Wiebe A, Riehl B, Lips S, Franke R, Waldvogel SR (2017) Unexpected high robustness of electrochemical cross-coupling for a broad range of current density. Sci Adv 3(10):eaao3920

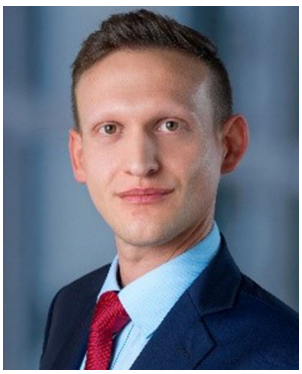

Maximilian Selt Maximilian Seltobtained his Bachelor of Science degree in Chemistry (2014) from the JohannesGutenberg University Mainz. After working there as undergraduate researchassistant (2014), he obtained his Master of Science degree in Organic Chemistry(2016) and his PhD degree (2020) under the supervision of Prof. Dr. S. R.Waldvogel working on electrochemical oxidative homocoupling reactions ofphenols. His doctoral studies were supported by a FCI scholarship and amembership in the MAINZ graduate school of excellence.

Barbara Gleede Barbara Gleedestudied chemistry at the Johannes Gutenberg University Mainz, where sheobtained her Bachelor of Science degree (2014) and her Master of Science degree(2016). She earned her doctorate degree (2020) in the field of anodic C,Ccross-coupling reactions under Prof. Dr. S. R. Waldvogel. Meanwhile she wasvisiting PhD student at Keio University (Eingaga group) in Japan and did aninternship at Novartis Pharma AG (Basel, Switzerland).

Robert Franke Robert Franke studiedchemistry at Bochum University. He earned his doctorate degree (1994) inrelativistic quantum chemistry under Prof. Dr. W. Kutzelnigg. After working asa research assistant, he joined the process engineering department (Hüls AG,the former company of Evonik Industries AG, 1998). He is now DirectorInnovation Management Hydroformylation and was awarded his habilitation (2002),since when he has taught at the University of Bochum. In 2011 he was madeadjunct professor. His research focuses on homogenous catalysis, processintensification, and computational chemistry.

Andreas Stenglein Andreas Stenglein received his degree asspecialist in mechanical engineering (Handwerkskammer Rheinhessen) in 1992.From 1992 - 2016 he was working as a specialist in mechanical engineering forthe mechanical workshop of the Institue of Organic Chemistry/JGU Mainz. In 2016he took the lead of all mechanical workshops which are located at theDepartment of Chemistry at JGU Mainz.

Siegfried R. Waldvogel Siegfried R.Waldvogel studied chemistry in Konstanz and received his PhD from University ofBochum/Max Planck Institute for Cole Research (Prof. Dr. M. T. Reetz, 1996).After postdoctoral research at Scripps Research Institute (Prof. Dr. J. Rebek,Jr.), he started his research career at University of Münster (1998). After hisprofessorship (University of Bonn, 2004) he moved to Johannes GutenbergUniversity Mainz (2010). His research interests are novel electro-organictransformation including bio-based feedstocks fromelectrosynthetic screening to scale-up. He co-founded ESy-Labs GmbH in 2018which is dealing with custom electrosynthesis and contract R&D.